Mon. Not. R. Astron. Soc. **349,** 1291–1322 (2004) doi:10.1111/j.1365-2966.2004.07600.x

The abundance distributions of Galactic bulge and disc planetary nebulae

K. M. Exter,[1,2,3,4★†] M. J. Barlow[4] and N. A. Walton[5]

[1]*Department of Physics and Astronomy, University of St Andrews, North Haugh, Fife*
[2]*N. Copernicus Astronomical Centre, ul. Bartycka 18, 00-716 Warsaw, Poland*
[3]*APS Division, Dep't Pure and Applied Physics, Queen's University Belfast, Belfast BT7 1NN*
[4]*Department of Physics & Astronomy, University College London, Gower Street, London*
[5]*Institute of Astronomy, University of Cambridge, Madingley Road, Cambridge*

Accepted 2004 January 5. Received 2003 December 30; in original form 2003 September 5

ABSTRACT

We present an abundance analysis of a sample of Galactic bulge planetary nebulae (GBPNe). The observational data set consists of spectra of 88 nebulae obtained with the FLAIR II multiobject spectrograph on the UK Schmidt Telescope, together with spectra of 42 nebulae obtained with the RGO Spectrograph on the Anglo-Australian Telescope. After selecting those for which reliable nebular electron temperatures could be derived, collisionally excited line abundances were derived for 45 GBPNe.

These were then compared with similarly derived abundances for 54 Galactic disc PNe (GDPNe), taken from the work of Kingsburgh & Barlow. We find that within the errors the abundances have the same average values, essentially the same distributions – including that for the mass-sensitive N/O ratio – and show the same relationships. The width of the nitrogen distribution exceeds that arising from errors, which could be a consequence of the range of precursor masses. The ratio of Type-I to non-Type-I PNe in the bulge and disc samples is similar, 18 and 25 per cent respectively. For the GDPNe, we find larger N/H and N/O ratios for the *small* number of those with He/H > 0.14, compared with those with He/H < 0.14.

For neither disc nor bulge sample is there any strong evidence for a depletion of oxygen for the higher-mass precursor stars (Type I PNe). We find no correlation between O/H and N/O or He/H. On the N/O to He/H plane, the bulge and disc PNe show a distribution whereby the low N/O values only occur for low He/H values, but at N/O > 0.25 the whole range of He/H values were sampled. The theoretical tracks to which we compare our data do not explain the PNe with low He/H abundance and high N/O ratio.

Realistic uncertainties in collisionally excited lines (CEL) abundances for individual PNe are quite large, of the order of 40 per cent for oxygen. Large samples are therefore required to get good statistical accuracy. This is usually achieved by combining many studies, and so we have compared the results of a number of published studies with our own, to search for any systematic differences. The average abundances are found to be the same within the errors except for cases where the abundance derivation methods are dissimilar, where systematic differences can occur. The N/O ratio is especially sensitive to the details of the abundance derivations.

Our bulge PN sample shows no evidence for either very-low-metallicity objects or for super-metal-rich objects – the implied mass and age distributions of the bulge PN precursor stars are indistinguishable within the observational errors from those in the local Galactic disc.

Key words: stars: abundances – planetary nebulae: general – Galaxy: abundances – Galaxy: bulge.

★Present address: IAC, c/Via Lactea, E38200 La Laguna (Tenerife), Spain.
†E-mail: katrina@ll.iac.es

1 INTRODUCTION

Planetary nebulae are those nebulae that surround the post-asymptotic giant branch (AGB) stars which originated from low–intermediate mass (LIM) main-sequence stars (e.g. Iben & Renzini 1983). They consist of a degenerate dwarf and a nebula made up of previous stages of mass loss. The abundances of some elements in these nebulae – such as O, Ne, Ar, and S – are unaffected by the preceding evolution and so reflect the chemistry of the interstellar medium (ISM) from which the stars formed, although the surface abundance of oxygen has been argued to have been altered in some objects, (see Péquignot et al. 2000). Other elements, for examples N and He (and C: not dealt with here), are affected by the AGB nucleosynthesis and dredge-up cycles, and so their abundances inform on the preceding evolution. A comparison of PN abundances in different part of the Galaxy can allow one to explore the relative chemical evolution history.

In this paper we concentrate on a comparison of abundances determined for a sample of GBPNe with those determined for GDPNe by KB94. The same abundance derivation methods have been used for the two samples, so minimizing the chances that systematic errors could bias the comparison.

In our study we separate the PNe into Type-I and non-Type-I classes. The Type I–IV classification system originated with Peimbert (1978), based on kinematical, spatial, morphological, and abundance criteria. All PNe are enriched in nitrogen and helium (Monk, Barlow & Clegg 1988) consistent with the operation of the first dredge-up (Becker & Iben 1979, 1980). Some PNe are particularly enhanced, and it has been suggested that these evolved from higher mass precursor stars, $M_{\rm zams} > 2.4\,{\rm M}_{\odot}$ (Peimbert & Serrano 1980), which have enhanced nitrogen production over the low-mass precursors. Peimbert's chemical criteria placed Type I PNe as those with $N/O > 0.5$ and $He/H > 0.125$. However, we adopt the slightly different definition developed by KB94. In the case of GDPNe with $N/O > 0.8$, they found no evidence for significant oxygen depletion, including those with high helium and nitrogen abundances. They argued that those with high observed nitrogen abundances are a result of CN-cycle envelope-burning conversion to nitrogen of primary carbon brought up by the third dredge-up; envelope-burning occurs only for higher mass cores. Type I PNe were thus defined as those having nitrogen abundances which exceed the sum of the original (ISM) C+N+O abundances for their galaxy, implying that the observed nitrogen must be primary and not secondary. This definition led to the criterion that a local disc Type I PN must have $N/O > 0.8$. We adopt the same for the bulge PNe, although we discuss the problems with this.

Three sets of GBPNe spectra have been used in this study. The measurement of the fluxes (Section 2), and derivation of the electron temperatures, densities and the abundances (Section 3), are discussed, as are errors and selection effects (Section 5 and the Appendices). The distribution functions and relationships between elements and element ratios are described in Section 4, and finally we compare our work to other studies of bulge and PN abundances (Section 6 and Section 7).

2 THE OBSERVATIONAL DATA SETS

2.1 The FLAIR II data

2.1.1 Observations and selection

U.K. Schmidt fields F456 and F455 were observed with the 1.2-m UK Schmidt Telescope over 4 nights in 1992 June, with the only overt selection criterion being to observe as many PNe as possible. We used the FLAIR II facility, a wide-field, multiobject spectrographic system. This system has not been much used for nebular studies, although Morgan & Parker (1998) used it to derive line ratios for PNe in the Magellanic Clouds. The FLAIR II facility has been described in detail by Watson et al. (1993) and Parker (1997) (see also http://www.aao.gov.au/ukst/flair.html).

FLAIR II was operated with 92 fibres of 100-μm diameter (6.4 arcsec projected onto the sky), which could be placed over a field of 40 deg^2; during our run a total of 153 PNe and 32 sky positions were observed. A number of the programme PNe have angular diameters slightly larger than the fibre size, but since absolute flux calibration was not carried out this was judged to be of little importance. Three gratings were used; 600V in two settings, 5400–6900 and 3600–5100 Å with a dispersion of ∼2.7 Å pixel^{-1}, 250B at 6.1 Å pixel^{-1} over 3700–7400 Å, and 1200B at 1.33 Å pixel^{-1} over 3600–4500 Å. Several astronomical exposures were taken in a sequence of varying exposure time, bracketed by arc spectra (Hg–Cd, Ne and He). Dome flat-field and bias spectra were taken at the end of each night. Details of the observations are given in Tables 1 and 2.

To minimize contamination by non-bulge PNe, a few selection criteria were applied post-observation. All with 5-GHz fluxes $\geqslant$100 mJy and those with optical diameters greater than 10–12 arcsec (corresponding to ∼0.5 pc at a bulge distance of e.g. 7.6 kpc: Maciel & Quireza 1999) were rejected, and as a secondary criterion those with a low radial velocity were double-checked for possible non-bulge status. The radio fluxes and nebular diameters were taken from Acker et al. (1992) and radial velocities from Durand, Acker & Zijlstra (1998). These selection criteria should have eliminated 90–95 per cent of non-bulge objects (Stasińska, Richer & McCall

Table 1. The log of FLAIR II observations.

Schmidt Field	Duration (s)	Grating	Seeing arcsec
	June 26 1992		
F456	600,300,600,712	250B −18.1°	∼2
	1200,1640,1800× 2		2–3
	120× 2,240,1800	600V −10.7°	1–2
	600, 1800	600V −14.5°	$\geqslant$ 2
	900		∼1
Dome Flat	5, 10, 60 × 2, 240	600V −14.5°	
	June 28 1992		
F456	1800× 4	600V −14.5°	1–2
	120,300,1800× 2	600V −10.7°	∼2
	600,1800× 3	1200B −7.4°	1–2
	1800		2–3
Dome Flat	240× 2	250B −18.1°	
	June 29 1992		
F455	60,300,1800× 2	250B −18.05°	1–3
	1800× 4	600V −14.5°	2–3
	1800		$\geqslant$ 3
	1800× 4	600V −10.7°	$\geqslant$ 4
	1800		$\geqslant$ 3
	1800		$\geqslant$ 2
	400		2–3
Dome Flat	300× 2,600	600V −10.7°	
	June 30 1992		
F455	1800 × 2	600V −14.5°	2–3
	3000 × 2		∼2
	300,900,1800	250B −18.1°	∼2
Dome Flat	300 × 2	250B −18.1°	

Table 2. The normal names, PNG or PK (xxx±x x) number (Acker et al. 1992), and comments (ours or from Acker et al.) for the FLAIR II observed PNe.

Name	PNG/PK	Comments	Name	PNG/PK	Comments	Name	PNG/PK	Comments
				Schmidt Field F456				
Ap 1-12	003.3−4.6		H 2-41	003.8−4.5		M 2-33	000.2−6.2	
Bl 3-10	000.1−2.3		H 2-43	003.4−4.8		M 2-37	004.2−5.9	
Bl 3-13	000.9−2.0		IC 4673	003.5−2.4		M 3-16	359.1−2.3	
Bl 3-14	000-1 4	possible PN	KFL 1	000.5−3.1		M 3-17	359.3−3.1	
Bl 3-15	000.6−1.3		KFL 2	002.2−2.5		M 3-19	000.4−2.9	
Bl M	001.3−1.2		KFL 3	359.7−4.4		M 3-20	002.1−2.2	
Bl O	000.8−1.5		KFL 4	003.0−2.6		M 3-22	000.7−3.7	
Bl Q	001.6−1.3		KFL 5			M 3-23	000.9−4.8	
H 1-40	359.7−2.6		KFL 9	359.9−5.4		M 3-26	004.8−5.0	
H 1-44	358.9−3.7		KFL 11	004.1−3.8		M 2-36	003.2−6.2	
H 1-45	002.0−2.0		KFL 12	003.2−4.4		M 3-45	359.7−1.8	
H 1-46	358.5−4.2		KFL 14	002.5−5.4	south	M 3-46	359.1−2.9	
H 1-47	001.2−3.0		M 1-37	002.6−3.4		M 3-47	000.3−2.8	
H 1-50	358.7−5.2		M 1-38	002.4−3.7		M 3-48	359.0−4.1	
H 1-54	002.1−4.2		M 1-42	002.7−4.8		M 3-51	358.6−5.5	
H 1-55	001.7−4.4		M 1-44	004.9−4.9		M 4-7	358.5−2.5	
H 1-56	001.7−4.6		M 2-19	000.2−1.9		NGC 6565	003.5−4.6	
H 1-60	004.2−4.3		M 2-20	000.4−1.9		Pe 1-12	004.0−5.8	
H 1-62	000.0−6.3		M 2-21	000.7−2.7		Pe 2-11	002.5−1.7	
H 1-63	002.2−6.3		M 2-23	002.2−2.7		Pe 2-12	002.8−2.2	
H 2-31	001.7−1.6		M 2-25	359.0−4.8		ShWi 2-1	001.4−3.4	
H 2-32	000.6−2.3		M 2-26	003.6−2.3		ShWi 2-2	358-3 5	possible PN
H 2-33	359.4−3.4	extended	M 2-27	359.9−4.5		ShWi 2-4	358-3 7	possible PN
H 2-34	001-2 1	symbiotic	M 2-28	000.3−4.6		ShWi 2-6	358-3 9	possible PN
H 2-37	002.3−3.4		M 2-29	004.0−3.0		ShWi 2-7	001.8−3.8	
H 2-37	002.3−3.4		M 2-30	003.7−4.6		SwSt 1	001.5−6.7	WR central
H 2-39	002.9−3.9		M 2-32	359.8−7.2				star, bulge PN?
H 2-40	000.1−5.6							
				Schmidt Field F455				
Th 3-24	357.1+1.9		Al 2-Q	000.5−1.6		H 2-30	357.9−3.8	
Th 3-26	358.8+3.0		Al 2-R	358.7−2.7		Hubble 5	359.3−0.9	foreground
Th 3-29	358+2 3	symbiotic	Al 2-S	001.1−1.6	Sa 3-92			central region
Th 3-30	59+2 1	symbiotic	Ap 1-1	357+2.1	not PN, no	K 1-4	001.0+1.9	not PN?
Th 3-32	359.4+2.3				emission lines	M 1-26	358.9−0.7	foreground
Th 3-33	359.8+2.4		Bl 3-3	001−0 2	no PN, no	M 1-27	356.5−2.3	
Th 3-34	356−0 1	possible PN			emission lines	M 1-29	359.1−1.7	
Th 3-35	359.3+1.4		Bl 3-5	358−0 1	M star?	M 2-16	357.4−3.2	
Th 3-55	356.5+1.5		Bl 3-10	000.1−2.3		M 2-18	357.4−3.5	
TrBr 4	357.6+1.0		Bl 3-11	001−0 1	symbiotic	M 2-19	000.2−1.9	extended
Wray 16-318	357-3 1	symbiotic?	Bl 3-14	000−1 4	possible PN	M 2-20	000.4−1.9	
Al 2-A			Bl 3-15	000.6−1.3		M 2-36	003.2−6.2	
Al 2-B	358.5+3.7		Bl B	358.3+1.2		M 3-16	359.1−2.3	
Al 2-D	357+2 8	not PN, no	Bl D	358.2−1.1		M 3-42	357.3+3.2	
		emission lines	Bl M	001.3−1.2		M 3-43	000.1−1.1	
Al 2-E	359+3 6		Bl O	000.8−1.5		M 3-44	359.3−1.8	
Al 2-F	358.5+2.9		Bl Q	001.6−1.3		M 3-45	359.7−1.8	
Al 2-G	359.0+2.8		H 1-17	358.3+3.0		M 3-46	359.1−2.9	
Al 2-H	357.2+1.4	double	H 1-18	357.6+2.6		M 4-4	357.0+2.4	
Al 2-I	359.6+2.2		H 1-19	358.9+3.4		M 4-6	358.8+1.8	
Al 2-J	000.1+2.6		H 1-20	358.9+3.2		M 4-7	358.5−2.5	
Al 2-K	359.5+2.6		H 1-23	357.6+1.7		Th 3-16	357.5+3.5	
Al 2-M	357−2 1	not PN, no	H 1-40	359.7−2.6		Th 3-19	358.4+3.3	
		emission lines	H 2-10	358.2+3.5		Th 3-20	357+2 3	symbiotic
Al 2-N		possible PN	H 2-13	359.1−2.3		Th 3-23	358.0+2.6	
Al 2-O	358.3−2.5		H 2-29	357.6−3.3				

1998) from our sample. Of the PNe with eventual abundances derived, we have additionally rejected as bulge objects Hubble 5, IC 4673, NGC 6565, M 1-29, M 1-26 and SuWt 1. M 2-29, previously identified as a halo PN, is now thought to be a bulge PN (Torres-Peimbert et al. 1997). Ground-based studies have yielded a very high electron temperature (Webster 1988; Peña Torres-Peimbert & Ruiz 1991; Ratag et al. 1997), but Torres-Peimbert et al. concluded, given their derivation from *HST* spectra of a more normal T_e of 9310 K for a spatially resolved knot in the nebula, that the former values may be affected by a very high-density region close to the star. We

therefore do not include this PN in our abundance analysis, although we do present our results without any correction for the high-density region.

2.1.2 Data reduction

Most of the data reduction was done within the IRAF[1] environment following procedures recommended by the UK Schmidt Unit.

The spectra lay in the long direction of the 578 × 420 pixel CCD, each spectrum being 3–4 pixels wide with nominally 1 pixel between spectra. After removal of the bias level, consecutive astronomical images of similar air-mass and exposure time were averaged together and cosmic-rays removed. Spectral flat-fielding, identifying and tracing the spectra on the CCD, correcting to a uniform fibre-efficiency, removing the scattered light, and extracting the spectra were carried out using the IRAFutility DOHYDRA. Wavelength calibration and sky subtraction were done with the STARLINK package FIGARO(Shortridge et al. 1999). Prior to sky-subtraction all the spectra were normalized to the flux of the [O I] 5577-Å sky line as measured on the average sky spectrum. For the short-wavelength spectra, which had no sky lines, a simple mean sky spectrum, or a fit thereto (at low signal-to-noise ratio: S/N) was subtracted. After sky subtraction, the appropriate spectra were then added together to leave one or two spectra of high and low S/N per PN per grating, the latter having the strongest nebular lines unsaturated.

Because the observations were made during an early run of FLAIR II, a number of non-optimum procedures were carried out during the observing run. It was therefore necessary to make some modifications to the recommended data reduction route. Full details are given in Exter (2000) and we only summarize here. The two main problems were (A) the fibres were too closely packed together, and (B) the flat-field exposures were taken each night at one grating setup only (that in place at the end of the night). The result of (A) is that for the brighter spectral lines, the wings of the emission-line profile can cross over beyond the fibre's boundary and into the next spectrum (a form of cross-talk), while (B) means that flat-field images for all of the grating setups observed during each night were not available. As these flat-field images are used to identify and trace the fibres, and to perform the spectral flat-fielding, a flat-field taken with the same grating set-up as the astronomical image should ideally be used.

2.1.2.1 ***Contamination problems (A)*** Tests done on sky spectra located adjacent to bright PNe spectra showed that, to within the errors of our measurements, the percentage of signal leaking from a bright spectrum did not depend on wavelength and occurred only for the brightest spectral lines for which it was obvious from looking at the raw spectral images that some overflow had occurred. The only trend was that the cross-talk was greatest at the four corners of the CCD, owing to defocussing effects.

For about 35 PNe, corrections derived from measurements of the raw extracted spectra could be applied to compensate for counts lost to, or gained from, an adjacent spectrum. If individual lines could not be corrected for, e.g. owing to blending, a correction factor derived from the rest of the spectrum (based on lines that could be corrected for) was used. About 5 PNe had to be discarded altogether. For the remaining ∼50 PNe, contamination may be present at about the 10–15 per cent level, where the effect of cross-talk from adjacent fibres was usually a problem only for the brightest lines; e.g. Hα, [N II] 6548, 6584 Å, [O III] 4959, 5007 Å.

2.1.2.2 ***Flat-fielding and fibre identification problems (B)*** For the spectra taken at the end of night, the correct flat-field images necessary for the reduction of the spectra were acquired immediately afterwards ('A' class images). For the rest ('B' class data), no flat-fields at the same grating setting were taken on the same night, so those from different nights had to be used. The main correction required to allow this was a small shift to the position of the spectra on the CCD, to account for the small movement of the fibres over the nights. The shifts ranged from <1 to 3 pixels and were determined by cross-correlating the relevant summed flat-field spatial spectra against each other. It was also necessary to extrapolate some of the flat-field spectra, by no more than 10 per cent of the total wavelength coverage, to account for slight grating angle differences.

To determine if these modifications adversely affected the quality of the spectra, we mimicked the modifications needed for the B class data reduction for the A class data too, and compared the counts in these extracted spectra with the correctly extracted ones. Generally, they were the same to ±3 per cent, with a few lines showing differences of up to ±10 per cent, but no systematic trends were found.

2.1.3 Relative flux calibration

It was not possible to observe spectrophotometric flux standard stars during the observing run, therefore an alternative to the usual calibration method was necessary. Since all measured line fluxes are ratioed to that of Hβ, absolute flux calibration was not necessary. For relative spectral flux calibration, we took advantage of the fact that many of the PNe observed had published line fluxes, measured from spectrophotometrically calibrated spectra. For a total of twelve PNe in F456 (M 1–42, M 2–27, H 1–47, M 1–37, M 3–46, H 2–32, M 2–29, M 2–23, M 2–30, H 1–40, H 1–54, and M 2–33), and five from F455 (H 1–23, H 1–20, Hubble 5, M 4–6, and M 1–29) we adopted means of the line fluxes relative to Hβ given by Webster (1988), Ratag (1990), Dopita et al. (1990), Aller & Keyes (1987) and Peña et al. (1991). These fluxes were divided into the line-count ratios measured from our own spectra. Low-order polynomial fits to the average ratios versus wavelength were then adopted as the calibration curves; one for each of the four wavelength and resolution settings. These corrections were then multiplied into all the spectra. To supplement the low number of standard nebulae for field F455, we compared the post-correction calibrated spectra for seven PNe that were in common with field F456; the agreement was very good.

2.1.4 Flux measurements and reddening estimates

Line fluxes were measured within the DIPSO(Howarth et al. 1998) environment, using the two routines FLUXand ELF. The former was used for most of the lines; it measures the total flux above a linearly interpolated continuum that is identified with a pair of cursor selections. ELFfits Gaussian profiles to the lines, and was chiefly used for blended or faint lines. For low S/N lines, the full-width at half-maximum of the Gaussian profiles was taken from that of nearby, bright isolated lines. For blended lines for which the individual centres could not be easily located, only the total flux was

[1] Image Reduction and Analysis Facility is distributed by the National Optical Astronomy Observatories, which is operated by the Association of Universities for Research in Astronomy, Inc. under cooperative agreement with the National Science Foundation (USA).

measured; none of these lines proved important in our subsequent analysis. Measurement errors are estimated by ELF while for lines measured with FLUX, multiple measurements varying the position of the continuum led to an error estimate. For the brightest lines (e.g. Hα, [O III] 4959, 5007 Å) the measurement errors are 1–5 per cent, and for the faintest, low S/N lines (e.g. He I 4921 Å, [O I] 6363 Å, [N I] 5200 Å) they are 20–40 per cent. For lines of intermediate S/N, errors are typically 10–15 per cent.

All measured fluxes were scaled to the Hβ flux, where F(Hβ) = 100. For red spectra that did not extend down to 4861 Å, F(Hα) from lower resolution spectra covering both Hα and Hβ was used as an intermediate scaling step. The value of the logarithmic extinction coefficient, c(Hβ), was calculated using the ratio F(Hα)/F(Hβ), or F(Hγ)/F(Hβ) if the spectrum did not extend to 6563 Å, compared with the theoretically predicted values for a nebula at an electron temperature of $T_e = 10^4$ K, and electron density $n_e = 10^4$ cm^{-3} (Hummer & Storey 1987) under Case B conditions using the Howarth (1983) Galactic reddening law and $R_v = 3.1$. This procedure also effectively corrects for any remaining wavelength-dependent instrumental effects on the spectra; the true values of c(Hβ) therefore cannot be obtained. Both values of c(Hβ) were used, with that from Hγ/Hβ for $\lambda < 4861$ Å unless the error was too large.

To obtain the final relative fluxes for each PN, the individual measurements for each line (i.e. from the different resolution and wavelength coverage spectra) were merged. The individual measurements were first scaled to those of the long-wavelength, low-resolution spectrum, which has the most accurate flux calibration. Weighting was applied in proportion to the errors. Fluxes for blended or faint lines were preferentially adopted from the high-resolution spectra, for bright isolated lines, from the low-resolution spectra.

A comparison of multiple measurements of individual lines measured from different spectra shows, for all except the lowest S/N lines, a scatter of ∼20 per cent.

2.2 The 1988 Middlemass data set

These observations were made with the 3.9-m AAT telescope in 1988 June. The RGO spectrograph with the 25-cm camera and the image photon counting system (IPCS) as detector were used, with the 1200 and 250 line mm^{-1} gratings, the latter with wide- (6.7 arcsec) and narrow-slit (1 arcsec) settings. Wide-slit observations of two photometric standard stars allowed for flux calibration. The selection criteria were that the central star spectrum be observable, resulting in a concentration to low-excitation PNe. The details of the original data reduction and flux measurements are given by Middlemass (1990), who reduced and measured the emission-line fluxes but did not analyse them to obtain abundances.

The data used were calibrated line fluxes measured from spectra with different wavelength ranges, resolutions, and exposure times for each PN. We combined the fluxes from sequences of exposures with the same slit-width, resolution and wavelength range, weighting by their exposure time, with an additional correction for the presence of neutral density filters. They were dereddened in the same manner as the FLAIR II spectra. The relative fluxes from the different slit-widths and wavelength ranges were then merged, using the same guidelines as for the FLAIR II data and with the widest slit spectrum being adopted as the most accurately calibrated reference spectrum.

The flux errors are slightly less than those for the FLAIR II data, since these AAT spectra are more reliably flux calibrated.

Table 3. Details of the AAT 1978 and 1986 observations.

Name	UTdate	Slit[a] (μm)	ND	Time (s)	Airmass
Hubble 8	8/10/78	134	–	800	1.56
	8/10/78	134	1.2	100	1.65
	8/10/78	134	2.1	100	1.68
	8/10/78	1000	2.1	100	1.70
	8/10/78	1000	1.2	100	1.72
	8/10/78	1000	0.62	400	1.74
	9/11/86	151	0.34	298	1.52
IC 4673	8/10/78	130	–	889	1.77
	8/10/78	2350	1.2	300	1.95
	8/10/78	1000	–	600	2.02
He 2-436	8/10/78	130	–	1000	1.64
	8/10/78	130	1.2	200	1.77
	8/10/78	1000	0.62	600	1.84
	8/10/78	1000	1.78	100	1.95
	8/10/87	1000	1.78	100	1.98
	9/10/78	1000	1.78	300	2.34
	8/11/86	180	–	330	1.44
	8/11/86	180	0.7	100	1.47
PC 14	26/8/78	100	0.34	500	1.45
	26/8/78	2140	2.1	150	1.49
	26/8/78	1000	1.2	500	1.53
Ae 1	26/8/78	150	–	600	1.26
	26/8/78	2300	0.62	200	1.31
H 1-63	26/8/78	150	0.62	400	1.47

[a]RGO Spectrograph 25-cm camera with sky projection factor of 6.7 arcsec mm^{-1}.

2.3 The AAT 1978 data set

The final spectra analysed were from observations made at the AAT in 1978 August/October and in 1986 November, with the RGO Spectrograph with the 25-cm camera and the IPCS (see KB94 for details), using the 250B grating with wide, medium and narrow slit widths. For flux calibration, spectra of the Oke standards L930-80 and VMa2 were taken. The 1986 spectra of Hubble 8 and He 2-436 were not flux calibrated and were used only to provide the intensity ratio of [O II] 3726/3729 Å for electron density calculations. The fluxes were measured by us in the same manner as for the FLAIR II spectra. Consecutive exposures were combined prior to measurement, dereddening was carried out using assumed Balmer line ratios, and the measurements from different slit-widths were then combined after scaling to those from the widest slit spectra. The formal measurement errors are the lowest of all the data sets; a few per cent, <10 per cent, and up to 30 per cent for the highest, mid and lowest S/N lines. A log of these observations is provided in Table 3. He 2-436 was rejected from our subsequent study as it is a member of the Sgr dwarf galaxy (Walsh et al. 1997), and IC 4673 and PC 14 were rejected, being foreground nebulae.

2.4 Dereddened fluxes

The final, dereddened fluxes for all our PNe are presented in Table 4. Only lines of importance to the abundance derivations are included, for the full list see Exter (2000). PNe included in more than one of our data sets have all measurements listed. It is stressed that the c(Hβ) values given are those calculated to produce agreement of the measured with the expected Balmer line ratios, and for the FLAIR II PNe may include some contribution from uncorrected instrumental response functions. It is generally accepted that the

Table 4. Dereddened line fluxes I(λ)/I($H\beta$) for our bulge Ne, on a scale where I(Hβ)=100.0. ':,::' indicate uncertain values. Superscripts indicate flux ratios taken from the literature or other comments.

	FLAIR II PNe											
	Al 2-E	**Al 2-F**	**Al 2-H**	**Al 2-I**	**Al 2-Q**	**Ap 1-12**	**Bl-Q**	**Bl3-15**	**H 1-17**	**H 1-18**	**H 1-19**	**H 1-20**
c(Hβ)	2.75	2.26	3.10	3.01	3.04	0.72	3.29	3.19	2.88	2.82	2.23	2.64
3727 [O II]	39.6*					13.6						
3835 H9									7.55			
3868 [Ne III]						6.69						86.2
3967 [Ne III],H7						9.98						
4101 Hδ						25.9						
4340 Hγ		46.5			46.5	46.5			46.5		46.5	46.5
4363 [O III]									25.6			
4471 [Ar IV]												
4686 He II	125		51.7	52.4	37.2							
4861 Hβ	100	100	100	100	100	100	100	100	100	100	100	100
4959 [O III]	562	465	299	593	341		378		504	459	134	333
5007 [O III]	1567	1394	906	1499	973		991		1488	1435	398	985
5200 [N I]	2:											2:
5517 [Cl III]					2.91	0.80						
5537 [Cl III]					24.7							
5755 [N II]							2.76		3.18	4.18	4.88	
5876 He I	6.97	15:	12.9	7::	14.7	0.94	14.2	11.9	14.7	14.0	16.7	15.1
6300 [O I]						1::	3::	10:	10.1	7.08		6.60
6312 [S III]									3.10	3.12		1.44
6363 [O I]	5.09						3::		3.39	3::		2.14
6435 [Ar V]				2::								
6548 [N II]	20.4		5:	7.86	15.2	74.9	34.0	116	21.8	78.8	73.0	55.3
6563 Hα	285	285	285	285	285	285	285	285	376	285	285	285
6584 [N II]	77.6	3.94	18.8	27.4	49.1	218	110	351	69.1	220	224	188
6678 He I	3.58		4.48	2:	4.17		4.67		4.07	6.57	5.56	5.32
6717 [S II]	8.05		7.65	3.60	6.86	8.02	7.43	20.2	2.33	6.11	4.51	8.39
6731 [S II]	9.36		5.60	4.97	7.44	14.7	12.0	26.7	4.75	14.2	6.05	13.3
7005 [Ar V]	5.45											
7065 He I	2.15	11.1	7::		3.93		5.19		12.5	11.1	10.4	9.94
7135 [Ar III]	17.2	11.5	11.2	16.6	15.7		23.5		27.2	35.7	27.3	32.6
7325 [O II]	4::		2:				5.15:		18.6	11.0	9.74	7.54
	H 1-23	**H 1-40**	**H 1-44**	**H 1-45**	**H 1-46**	**H 1-47**	**H 1-50**	**H 1-54**	**H 1-55**	**H 1-56**	**H 1-62**	**H 1-63**
c(Hβ)	2.72	2.56	1.92	2.57	1.51	1.10	0.70	1.05	0.43	0.89	0.64	0.72
3727 [O II]			87::		67::	37.5	45.1	92.6	76.1^{+}	24.8*	49.0	85.4
3750 H12								3.96				
3770 H11								4.35				
3798 H10								4.18			5.24	
3835 H9								7.55		5.16	2.76	
3868 [Ne III]		80.8		87.2	22.7		168	21.2		37.7		27.5
3889 H8,He I			57.0		12.0		22.6	16.8		19.5	9.23	
3967 [Ne III],H7				32.6	19.1		26.3	15.6		15.5	10.1	23.3
4026 He I								2.81		4.47		
4076 [S II]								1.29				
4101 Hδ			25.9	25.9	25.9	25.9	25.9	25.9		25.9	25.9	25.9
4267 C II											0.9:	
4340 Hγ	46.5	46.5	46.5	46.5	46.5	46.5	46.5	46.5	46.5	46.5	46.5	46.5
4363 [O III]		<21.4		$75.9^{!}$	4:		17.0	2.09		1.36		4.76
4471 [Ar IV]					5.54			4.69		4.68		1.74
4686 He II				25.4			11.5					
4711 [Ar IV]							2.97	0.6:				
4740 [Ar IV]							7.42					
4861 Hβ	100	100	100	100	100	100	100	100	100	100	100	100
4959 [O III]	406	348	36.0	290	162		558	150	4.30^{+}	189		134
5007 [O III]	1235	979	103	816	500		1740	460	12.1^{+}	580		399
5200 [N I]											1.13	
5517 [Cl III]			2.91	0.80				0.15				
5537 [Cl III]			24.7					0.35				
5755 [N II]	1::		1.54	0.90	1.54	0.40	2.00	2.13			0.65	3.68
5876 He I	15.7	14.1	15.2	17.7	13.5	0.82	12.6	13.1	6.32	13.0	1.60	10.8

Table 4 – *continued*

	H 1-23	**H 1-40**	**H 1-44**	**H 1-45**	**H 1-46**	**H 1-47**	**H 1-50**	**H 1-54**	**H 1-55**	**H 1-56**	**H 1-62**	**H 1-63**
6300 [O I]	3.31			0.8::	2:	0.71	10.9	2.36	<5		1.61	1.46
6312 [S III]	1.71			1.31	2:		2.29	1.46		0.47	0.1:	2.35
6435 [Ar V]						0.91						
6363 [O I]	0.60				0.47	0.38	2.67	0.96			0.30	0.43
6548 [N II]	25.4	15.9	102	1.34	14.4	67.7	21.0	28.5	79.4	4.23	69.6	12.9
6563 Hα	285	285	285	285	285	285	285	285	285	285	285	285
6584 [N II]	82.0	51.7	314	4.84	44.7	202	63.6	80.6	280	13.2	205	41.5
6678 He I	5.02	4.79	3.71	5.02	3.57	0.48	4.76	4.51	1.61^{+}	4.29	0.66	2.62
6717 [S II]	4.97	2.79	8.47		1.24	8.38	5.72	1.49	13.6	1.12	11.3	0.7::
6725 [S II]												
6731 [S II]	8.04	3.38	13.5		2.13	16.2	9.18	3.13	22.4	1.57	21.8	1::
7065 He I	8.61	13.4	3.82	22.7	9.69		3.99	11.0		5.35	0.6:	8.61
7135 [Ar III]	26.1	20.1	9.96	3.56	10.25		17.1	13.8	3.10^{+}	15.1	0.6:	11.3
7325 [O II]	5.91	14.6	2.00[#]		27.7		8.43	43.1	1.55^{+}	<2.3		58.9
	H 2-10	**H 2-13**	**H 2-29**	**H 2-31**	**H 2-32**	**H 2-33**	**H 2-34**	**H 2-39**	**H 2-40**	**H 2-41**	**H 2-43**	**Hubble 5**[a]
c(Hβ)	2.32	2.74	1.74	3.20	1.90	2.05	2.86	1.38	0.79	0.81	1.32	1.69
3727 [O II]				102::					137	92.0		76.4
3868 [Ne III]									68.4	52.2		78.6
3889 H8,He I										13.9		14.5
3967 [Ne III],H7									42::	25.5	42:	45.8
4026 He I										4.48		3.26
4068 [S II]										12:		9.44
4076 [S II]												3.19
4101 Hδ						25.9			25.9	25.9	26:	25.9
4267 C II										2.93		
4340 Hγ	46.5	46.5	46.5		46.5	46.5	46.5	46.5	46.7	46.5	47:	46.5
4363 [O III]							30.3	19.1		5::		26.5
4471 He I										6.85		3.69
4686 He II					72.1		43.6	39.1		31.6		54.5
4711 [Ar IV]								4:				10.1
4725 [Ne IV]												2.75
4740 [Ar IV]							5:				13.7	
4861 Hβ	100	100	100	100	100	100	100	100	100	100:	100	100
4959 [O III]	337	526				181		438	185	157	9:	610
5007 [O III]	1062	155	80.1			481	16:	1286	549	464	22:	1759
5200 [N I]									10.7		5:	8.20
5411 He II												4.43
5517 [Cl III]												0.96
5537 [Cl III]												1.65
5755 [N II]				3::	3.60				5.63	1.31		12.8
5876 He I	13.4	12.9	14:	2.39	3.59	14.4	11.1	9.14	13.3	15.3	14.0	11.5
6300 [O I]	0.65	5.23			4.10				17::			36.9
6312 [S III]	0.81	1.67			2.75							3.53
6363 [O I]	0.3::				0.92		0.50		3::			10.63
6435 [Ar V]												2.26
6548 [N II]	6.6	20.8	55.7	84.0	19.0	4.35			168	13.5	8:	236
6563 Hα	285	285	285	285	285	285	285	285	285	285	285:	285
6584 [N II]	19.2	66.2	141	263	59.7	19.1	3.40	7.10	537	37.2	14:	744
6678 He I	3.66	4.01	6:	1.95		5.42	3.88	2.74	3.59	6.46	7:	4.28
6717 [S II]	2.04	8.28		9.42	7.96	2.54		1.77	65.1			21.1
6725 [S II]			27.9									
6731 [S II]	2.8	13.1		16.1	10.1	3.24		1.32	51.7			33.4
7005 [Ar V]												7.20
7065 He I	6.00	5.77			2.17		7.83	2.47	1.91	2.72	9:	7.16
7135 [Ar III]	9.13	20.8	8.13		2.94	12.2		5.37	26.7	14.1		69.5
7325 [O II]	7.58	11.3			42.9					12.1		39.2
	IC 4673[a]	**K 1-4**	**KFL-01**	**KFL-03**	**KFL-05**	**KFL-09**	**KFL-12**	**M 1-26**[a]	**M 1-27**	**M 1-29**	**M 1-37**	**M 1-42**
c(Hβ)	1.32	1.23	1.68	1.25	1.76	1.09	1.76	1.08	2.23	2.27	1.14	0.50
3727 [O III]	26.9[&]			28.8				109	83.1	75.8	13.8	60.6
3750 H12								1.80				2.17
3770 H11								3.17				2:

Table 4 – *continued*

	IC 4673[a]	K 1-4	KFL-01	KFL-03	KFL-05	KFL-09	KFL-12	M 1-26[a]	M 1-27	M 1-29	M 1-37	M 1-42
3798 H10								5.47				4.00
3835 H9				5:				7.19	16.9			6.51
3868 [Ne III]	124			57.1		53.8				116		67.4
3889 H8,He I				11.4				107	14.0		9.26	19.7
3967 [Ne III],H7	41.2			19.2				15.7	10.6	43.8	13.1	28.5
4026 He I								0.80				3.26
4068 [S II]				5::				4.37				
4076 [S II]								1.29				
4101 Hδ	25.9			25.9		25.9	25.9	25.9	25.9	25.9	25.9	25.9
4340 Hγ	46.5		47:	46.5	46.5	46.5	46.5	46.5	46.5	46.5	46.5	46.5
4363 [O III]	10.5			12:	45.3[$]	17.3				9.23		2::
4471 He I	5.86							2.10		4.80		7.03
4686 He II	65.8		38:	13.4	31.40	106				34.0		11.2
4711 [Ar IV]						6.5				5.19		2.07
4740 [Ar IV]	5.82									4.88		1.22
4861 Hβ	100	100	100	100	100	100	100	100	100	100	100	100
4959 [O III]	386	300	257	201	301	208	338	24.2		484		156
5007 [O III]	1079	922	783	567	912	622	1000	72.9		1331	1.02	459
5200 [N I]										1.86	1.78	2.51
5411 He II	6.13									1.62		0.93
5517 [Cl III]										0.77		0.42
5537 [Cl III]	2.23							0.46		0.85		0.38
5755 [N II]	0.5::	5::			4.60			4.64		3.15	0.75	2.26
5876 He I	9.52	13.7	11.2	12.0	10.1	3.44	13.3	9.05	1.18	14.5	1.32	16.9
6300 [O I]				13::	7.52			3.47	3.16	7.88	1.46	2.76
6312 [S III]	2.58							2.45		3.42		1.06
6363 [O I]		12.9						1.12		2.52	0.56	1.26
6435 [Ar V]					3.92	0.63				0.51		0.10
6548 [N II]	11.5	162		37.5	14.9			71.6	60.1	106	78.3	72.0
6563 Hα	285	285	285	285	285	285	285	285	285	285	285	285
6584 [N II]	36.9	535	26.2	119	56.3	4.28	9.28	204	188	330	244	214
6678 He I	3.42	3::	5.37	5.47		1.57	4.34	3.48		4.53	0.84	6.52
6717 [S II]	6.27	49.2	3.58	18.1		0.9::		2.14	11.4	20.1	7.21	16.0
6731 [S II]	8.18	39.6	7.34	15.0		1:		4.27	19.2	34.3	14.0	18.9
7005 [Ar V]	1.69									1.59		
7065 He I	2.22		2.45	4.89	6.39		4.28	9.33		7.05		5.29
7135 [Ar III]	39.8	17.2	4.29	19.6	16.6	6.41	10.1	14.6		48.8		21.9
7325 [O II]	2.1[&]							135	3.29	11.43	2::	4.26

	M 1-44	M 2-19	M 2-20	M 2-23	M 2-25	M 2-26	M 2-27	M 2-28	M 2-29	M 2-30	M 2-32	M 2-33
c(Hβ)	0.81	1.15	1.80	1.20	1.10	1.81	1.65	1.44	1.05	0.92	0.34	0.65
3727 [O III]	29.7	206	88.3	16.7	183		49.7	151	42.1	12.5[&]		27.7
3750 H12				2.78								
3770 H11				3.69								3.98
3798 H10	5.43			4.70								4.57
3820 He I				1.58								
3835 H9	8.37			5.60				12.5			8.13	6.15
3868 [Ne III]				94.0	47.7	118::	75.8	84.5	49.8	50.8	120	31.3
3889 H8,He I	13.1	22.7	20.7	14.0	14.5		13.8	25.3	21.9	12:	21.6	18.9
3967 [Ne III],H7	4.49			44.7	25.7	46::	36.2	33.3	14.6	34.4	51.1	16.7
4026 He I				1.97	24.0				6.28		4.06	3:
4068 [S II]				2.08								
4076 [S II]				0.92								
4101 Hδ	25.9	25.9	25.9	25.9			25.9	25.9	25.9	25.9	25.9	25.9
4267 C II	4.01						8::	5.92				
4340 Hγ	46.5	46.5	46.5	46.5	46.5	46.5	46.5	46.5	46.5	46.5	46.5	46.5
4363 [O III]				13.0			4::	4.56	14.0	10.2	13.7	
4471 He I			6.46	5.13	3.60		4.63	5.54	5.72		4.46	4.31
4686 He II		14.7			23.8	20.9	2::	16.9		26.3	2.54	
4711 [Ar IV]				1.22							2.33	
4740 [Ar IV]				0.98							3.07	
4861 Hβ	100	100	100	100	100	100	100	100	100	100	100	100
4959 [O III]		50.7	181	383	247	198	278	216	146	424	373	197

Table 4 – *continued*

	M 1-44	M 2-19	M 2-20	M 2-23	M 2-25	M 2-26	M 2-27	M 2-28	M 2-29	M 2-30	M 2-32	M 2-33
5007 [O III]		131	520	1187	709	605	888	665	424	1307	1138	575
5200 [N I]					7.27		1.22	5.43				
5411 He II					2.02							
5517 [Cl III]	2.10			0.28			0.1:	0.79				
5537 [Cl III]				0.34			0.48	0.87				0.5:
5755 [N II]		1.04	0.56	1.08	3.82	1.81	1.97	3.70				
5876 He I	7.03	11.9	16.6	11.2	13.1	15.1	15.6	17.9	14.2	10.1	13.6	12.3
6300 [O I]		2.33	2.35	3.01	26.4	1.81	4.32	7.03	1.11			0.60
6312 [S III]		0.61	1.36	1.66	1.20		1.51	1.31	0.81		0.6:	
6363 [O I]		0.67	0.44	0.97	8.96	1.01	1.36	2.82	0.26			
6548 [N II]	71.7	58.2	38.7	6.85	134	75.4	46.8	152	6.91			3.80
6563 Hα	285	285	285	285	285	285	285	435	285	285	285	285
6584 [N II]	210	178	116	17.7	418	230	146	435	20.8	14.0	1.55	11.4
6678 He I	2.64	4.08	5.08	4.14	4.06	4.48	5.62	5.27	4.57	3.65	4.00	3.98
6717 [S II]	13.2	19.9	5.51	0.70	72.7	17.3	5.51	32.2	1.87	2.07	0.52	0.79
6731 [S II]	19.1	23.2	9.43	1.29	67.5	18.6	10.0	43.0	2.41	2.86	0.68	1.09
7065 He I	3.71	3.17	7.48	14.8	3.63	4.80	12.5	5.09	6.25	3.26	5.43	3.92
7135 [Ar III]		9.86	26.3	14.0	30.3	20.4	28.9	31.1	12.5	23.4	7.52	10.9
7325 [O II]		3.10	6.35	21.2	13.2		4.94	3.78	2.51	1.72[&]		2:
	M 2-36	**M 2-37**	**M 3-16a**	**M 3-16b**	**M 3-17**	**M 3-19**	**M 3-22**	**M 3-23**	**M 3-26**	**M 3-42**	**M 3-44**	**M 3-45**
c(Hβ)	0.73	0.92	1.59	1.72	3.24	1.36	0.95	1.47	0.84	1.80	3.86	2.60
3727 [O II]	45.9	55.7	123	178			35.2		22::			
3750 H12	2.53											
3798 H10	3.82											
3820 He I	2::											
3835 H9	6.27											
3868 [Ne III]	56.3		34.1	57.9		47.5	66.8	92.8	54.1			
3889 H8,He I	13.8	26.8					13.8		14.0			
3967 [Ne III],H7	22.0			19.2		25.2	26.4	26.3	24.0			
4026 He I	4.44											
4068 [S II]	4.36								7.26			
4076 [S II]	2.81											
4101 Hδ		25.9	25.9	25.9		25.9	25.9	25.9	25.9			
4267 C II	1.18		10::				2.27		5.57			
4340 Hγ	46.5	46.5	46.5	46.5		46.5	46.5	46.5	46.5	46.5	46.5	47:
4363 [O III]	2.26	6.40					17.8		4.63			
4471 He I	5.65	8.21						22.3	5.64			
4686 He II	2.49						102	89.2	26.9	68.2		29.9
4711 [Ar IV]							10.2	14.9	3.48			
4725 [Ne IV]							3.64					
4740 [Ar IV]	1.16						12.3	10.6	1.79			
4861 Hβ	100	100	100	100	100:	100	100	100	100	100	100	100
4959 [O III]	268	16.2	227	231	44:	156	279	404	194	520		555
5007 [O III]	787	45.7	662	655	91:	482	774	1222	563	1513		1735
5200 [N I]	1.21											
5411 He II	0.17							7.58				
5517 [Cl III]	0.31							0.70				
5537 [Cl III]	0.54							0.62				
5755 [N II]	1.81								0.78	2.56		
5876 He I	15.1	14.5	13.2	11.9	17:	16.7	2.32	4.53	15.8	6.15	3:	10.4
6300 [O I]	6.83	3::	2.20	1.92							7.32	4.72
6312 [S III]	1.41		1.18						0.6:			
6363 [O I]	2.57	0.69	0.81	0.5::								
6435 [Ar V]							1.49	1.98				
6548 [N II]	46.0	55.1	16.9	19.0	44:	6.40		6.13	4.65	96.9	60.7	13.2
6563 Hα	285	285	285	285	285:	285	285	285	285	285	285	285
6584 [N II]	141	160	55.4	59.8	152:	21.0		20.2	16.9	318	202	32.3
6678 He I	5.42	5.26	4.07	4.28	4::	5.89	1.69	2.18	5.16	2.55		4.07
6717 [S II]	10.0	16.0	7.14	8.11	9:		1.84	4.02	1.79	35.0	12.1	4.14
6731 [S II]	16.5	15.2	8.41	9.14	11:		1.98	4.89	2.53	41.0	19.7	5.70
7005 [Ar V]							1.41	4.54		5.46		
7065 He I	7.76	3::	3.32	4.42		3.43		1.18	3.03	4.51		

Table 4 – *continued*

	M 2-36	M 2-37	M 3-16a	M 3-16b	M 3-17	M 3-19	M 3-22	M 3-23	M 3-26	M 3-42	M 3-44	M 3-45
7135 [Ar III]	28.9	5::	11.2	11.7	5::	15.4	6.15	29.2	14.4	56.8		4::
7325 [O II]	9.80	4::	6.01	5.51	4::	5.34			5.95	6.00#		4.20#

	M 3-48	M 3-51	M 4-6	NGC 6565[a]	Pe 1-12	ShWi 2-1	SwSt-1[a]	Th 3-16	Th 3-19	Th 3-20
c(Hβ)	1.67	1.14	2.67	0.73	0.73	1.46	0.42	1.83	2.61	3.13
3727 [O II]		64.9	69.7	261			49.4			
3750 H12				2.03			2.38			
3770 H11				3.09			3.31			
3798 H10				3.70	39.3		4.61			
3820 He I							0.69			
3835 H9				4.83			6.48			
3868 [Ne III]				95.0						
3889 H8+He I				15.9			12.4			
3967 [Ne III],H7			19.3	47.4	19.3		15.3			
4026 He I				1.89			1.05			
4068 [S II]				7.07			3.84			
4076 [S II]				2.36			0.99			
4101 Hδ		25.9	25.9	25.9	25.9		25.9			
4267 C II				0.44			0.70			
4340 Hγ		46.8	46.5	46.5	46.5		46.5		47:	46.7
4363 [O III]		7.20		8.39	12.6		0.44		27:	
4471 He I		7.45		5.02			2.24			
4686 He II		30.7	15::	16.2	102	63.0	0.74		31.0	
4707 [Ar IV]									11.8	8.15
4711 [Ar IV]				2.14			0.46			
4740 [Ar IV]				1.29			0.4:			
4861 Hβ	100	100	100	100	100	100	100	100	100	100
4959 [O III]	234	190	273	379	200	157	11.9		599	
5007 [O III]	671	571	829	913	596	486	37.0		1800	
5200 [N I]				5.24						
5411 He II				1.21	4.02					
5517 [Cl III]				0.85			0.08			
5537 [Cl III]				0.84			0.27			
5755 [N II]	5.12	2.57	2::	6.42			5.81			
5876 He I	12.8	14.6	10.8	13.0	4.84	13.7:	6.34		11.6	4.7
6300 [O I]	19.4		6:	22.3			1.87		11::	
6312 [S III]			2.26:	3.02			3.08			
6363 [O I]	6.14		3:	202			0.54		6.3	
6548 [N II]	207	66.2	20.2	154	1.99	9.48	46.4	27.9	13.8	
6563 Hα	285	285	285	285	285	285	285	285	285	285
6584 [N II]	646	216	63.0	458	6.14	47.2	149	96.4	37.7	
6678 He I		4.91	4.17	4.52	2::	5.86	1.94		6.17	1.87
6717 [S II]	59.2	24.6	4.29	42.7		10:	0.80	18.0		1::
6731 [S II]	60.6	21.7	7.26	57.5		7:	1.94	20.2		1::
7005 [Ar V]									3.14	
7065 He I			9.02	5.16			8.05		13.1	
7135 [Ar III]	28.9	20.4	20.9	34.5	13.4		12.1		23.3	
7325 [O II]			21.7	22.8	9::		112		28.4	

	Th 3-26	Th 3-29	Th 3-30	Th 3-34		Th 3-26	Th 3-29	Th 3-30	Th 3-34
c(Hβ)	2.20	3.86	3.91	1.40	6563 Hα	285	285	285	285
4340 Hγ	46.8	46.8	47:		6584 [N II]	122	7::		138
4686 He II	65.9				6678 He I	3.68	7.53	8.18	
4861 Hβ	100	100	100	100	6717 [S II]	9.55			47.0
4959 [O III]	434				6731 [S II]	12.9			32.5
5007 [O III]	1269	30.5			7005 [Ar V]	2.84			
5411 He II	4.09				7065 He I	3.94	6.61	9.62	
5876 He I	8.1	13.8	14.5		7135 [Ar III]	32.0			
6548 [N II]	38.6	8::		42.2	7325 [O III]	6.42			

Middlemass PNe

	Al 1-1	Cn 1-5	H 1-20	H 1-35	H 1-42	H 1-53	H 1-54	H 1-55	H 1-60	H 1-63	KFL-01	KFL-03
c(Hβ)	0.41	0.98	1.56	1.46	0.58	1.75	0.97	1.19	1.16	0.37	0.77	1.63
3426 [Ne V]	427											
3726 [O II]		78.0	21.6	41.1	19.5	10.2	43.5	46.6	4.50	21.4	7.35	47.3
3729 [O II]		38.3	4:	15.8	9.30	4.20	21.6	23.5	2.13	7.74	7.39	53.7

Table 4 – *continued*

	Al 1-1	Cn 1-5	H 1-20	H 1-35	H 1-42	H 1-53	H 1-54	H 1-55	H 1-60	H 1-63	KFL-01	KFL-03
3750 H12		3.33		2.94	1.94	1.71	1.94	2.59	1.91	2.82	2.02	
3760 O III	3.68								0.60		3.19	
3770 H11	4.01	2.90		2.34	3.18	2.64	2.96	2.31	1.72	2.95	2.51	
3798 H10	5.36	3.87		4.56	4.05	3.69	4.52	4.16	2.74	3.73	3.26	4.77
3820 He I		2.00		0.71	1.25	0.94			0.84			1.68
3835 H9	6.63	7.26		6.38	6.75	5.34	5.06	4.76	3.44	4.28	6.25	7.42
3868 [Ne III]	62.2	80.3	64.3	22.3	81.2	76.5	12.9		47.5	12.4	55.8	62.0
3889 He I,H8	15.0	21.5	15.8	12.6	17.4	10.1	12.1	11.1	12.7	9.65	12.8	17.1
3967 [Ne III],H7	10.8	24.6	18.1	7.52	21.5	4.71	4.48	11.8	12.4	4.20	13.6	20.5
3970 H7	15.4	16.0	7.58	15.4	12.5	11.5	6.97		9.42	10.2	10.3	11.1
4026 He I	2.02	2.76		1.98	2.61	2.81	1.75		1.94	1.66	2.10	2.33
4068 [S II]		4.92	10.1	2.26	1.22	7.30	1.90		1.16	2.61	2.33	4.73
4076 [S II]		2.16		0.73		2.35				0.96	1.57	4.19
4097 N III					0.66						2.55	
4101 Hδ	26.0	24.8	22.6	27.4	27.3	26.2	21.2	34.0	26.6	23.8	19.9	22.8
4267 C II	1.06	1.15	1.90	0.14		0.94		0.55			5.56	
4340 Hγ	46.9	46.9	46.9	47.2	46.9	54.3	42.6	58.2	46.9	46.9	46.9	46.9
4363 [O III]	27.7	3.57		2.61	6.81	3.27	2.19		5.43	3.29	4.07	
4471 He I		7.68	9.93	5.63		8.93	3.02		8.98	3.01		
4645 N III,C III		52.4										
4658 C IV				3.26		5.31				2.70		
4686 He II									3.45			
4861 Hβ		100	100	100		100	100	100	100	100		
4959 [O III]		279	313	180		271	141	3.36	370	146		
5007 [O III]		1025		586		819	415	11.1				
5200 [N I]		2.96						2.25				
5517 [Cl III]				1.61								
5755 [N II]		3.53		2.16		7.04	1.58	1.20		2.38		
5876 He I		20.2	14.1	15.9		17.2	14.0	7.39	14.4	12.0		
6300 [O I]		4.97		2.22			3.91	2.43				
6312 [S III]							2.12					
6363 [O III]							0.78					
6548 [N II]		116	50.6	14.2		57.2	22.8	82.1		12.2		
6563 Hα		310	285	285		285	285	285	289	285		
6584 [N II]		315	159	43.8		212	51.9	220		34.5		
6678 He I		8.29	3.99	2.66		3.77	3.58		4.90	4.44		
6717 [S II]		11.7	5.06			1.57	1.88	6.38				
6725 [S II]				1.63								
6731 [S II]		22.4	9.78			2.93	2.16	10.26				
7065 He I		4.31	4.38	7.10		7.24	6.54	1.46		8.04		
7135 [Ar III]		26.7	16.9	9.58		27.0	7.54	2.58	18.3	7.68		
7325 [O II]		10.1	4.24				23.7			34.4		

	KFL-05	KFL-16	M 1-25	M 1-27	M 1-29	M 1-30	M 1-35	M 1-38	M 1-42	M 2-11	M 2-16	M 2-20
c(Hβ)	1.13	0.92	1.46	1.53	1.51	0.91	1.28	0.85	0.56	0.92	2.20	1.69
3426 [Ne V]	353	64.1			72.1					112		
3444 O III	14.0				22.7				7.68	10.4		
3726 [O II]		19.0	67.0	56.0	73.4	59.4	26.5	56.9	38.5	70.4	38.6	78.6
3729 [O II]		14.3	31.6	30.1	40.0	31.7	16.2	27.3	28.8	43.5	20.1	38.3
3750 H12	3.84		3.47		4.87	2.92	3.01	3.24	2.59	2.13	2.90	4.03
3760 O III	3.91				6.32				1.06	2.43	1.93	
3770 H11	2.59	4.36	4.06	2.47	5.75	3.79	3.67	4.37	3.26	2.55	4.11	8.68
3798 H10	3.74	4.08	5.31	5.12	5.15	4.36	4.13	3.86	5.07	3.89	6.76	
3820 He I			2.02			2.90	2.18		1.69		2.62	
3835 H9	4.39	5.15	9.24	4.85	5.61	5.95	8.93	4.10	7.35	5.16	6.91	7.83
3868 [Ne III]	238	62.5	6.27		168	4.94	68.8		66.0	139	113	16.0
3889 He I,H8	13.5	11.6	19.1	10.2	17.0	21.1	17.2	10.5				
3967 [Ne III],H7	70.2	11.6	2.03		43.9		7.47		21.2	24.3	23.4	2.05
3970 H7	5.96	14.2	11.7		12.7	6.20	14.4	9.41	10.7	14.5	16.2	20.6
4026 He I			2.45		3.45	4.21	4.62		4.07	2.89	3.18	
4068 [S II]	4.40	4.91	4.77	4.16	6.74	2.55		3.69	4.31	5.36	6.04	5.00
4076 [S II]			1.84						2.65	1.46		3.01
4097 N III		2.83			1.94	1.11	1.65		3.65	1.07	1.67	
4101 Hδ	24.7	25.6	26.4	25.0	26.3	24.0	30.1	26.8	28.3	23.9	25.8	33.1

Table 4 – *continued*

	KFL-05	KFL-16	M 1-25	M 1-27	M 1-29	M 1-30	M 1-35	M 1-38	M 1-42	M 2-11	M 2-16	M 2-20
4267 C II	1.20	2.66			1.24		1.64		2.88		0.53	1.51
4340 Hγ	46.9	46.9	47.4	46.7	44.5	47.8	51.6	47.0	46.9	46.9	46.9	57.4
4363 [O III]	81.1[@]	8.18	1.89		12.1	0.7:	2.17	1.25	2.65	31.8	3.93	1.31
4471 He I			5.99			8.68	12.5					6.45
4645 N III,C III			31.2									30.1
4658 C IV												31.8
4861 Hβ			100	100	100	100	100	100				100
4959 [O III]			156		613	42.5	246					186
5007 [O III]			533		1832	149	779					
5200 [N I]					6.87							
5517 [Cl III]												1:
5537 [Cl III]												3.99
5755 [N II]					7.38	4:	5.12	1.49				1.35
5876 He I			17.8		13.6	16.8	23.6	1.16				14.1
6300 [O I]			2.48		7.36			1.56				1.83
6312 [S III]			1.76									
6548 [N II]			66.7	64.5	112	83.8	55.7	57.7				36.2
6563 Hα			285	285	285	285	285	285				285
6584 [N II]			213	186	300	272	148	167				103
6678 He I			4.02		4.20	3.74	7.56					3.46
6717 [S II]			4.20	6.51	14.3	4.58	6.60	7.20				2.70
6731 [S II]			8.21	12.3	18.1	6.11	9.22	13.35				4.48
7065 He I			5.91		4.51	4.10	9.77					3.89
7135 [Ar III]			18.4		21.6	10.3	22.8					12.5
7325 [O II]			6.97	3.33	3.76	2.00		3.58				5.32

	M 2-21	M 2-22	M 2-23	M 2-27	M 2-30	M 3-20	M 3-21	M 3-7	M 3-8	M 4-3	PC 14	Vy 2-1
c(Hβ)	0.89	2.02	0.66	1.41	1.07	1.00	0.54	1.36	1.20	1.25	0.63	0.63
3426 [Ne V]	1.63				6.62							
3444 O III	12.0				14.1							
3726 [O II]	15.0	49.3	6.35	19.8	4.46	20.0	22.5	45.2	46.8	22.2	48.3	60.1
3729 [O II]	7.05	33.2	3.06	10.3	2.56	8.56	10.2	21.8	34.5	9.31	29.7	30.9
3750 H12		2.88	2.61	3.26	1.95	3.66	3.19			2.54	3.10	2.75
3760 O III	2.17	3.33			2.96						0.58	
3770 H11	3.67	4.19	2.54	2.63	1.93	3.00	3.33	1.84		4.68	4.30	4.07
3798 H10	4.35	6.27	2.73	3.90	2.87	5.05	4.61	4.37	6.01	2.14	6.07	5.87
3820 He I	0.89		1.26	1.31	0.69		1.48	1.75			1.99	1.60
3835 H9	6.35	7.35	4.64	6.01	4.87	6.65	6.12	6.87	8.19	5.25	9.16	8.22
3868 [Ne III]	82.7	88.7	83.6	83.6	66.0	117	153	18.9	31.0	50.0	104	50.2
3889 He I,H8					12.0	21.6	13.2	20.4	22.7	12.7	26.7	21.77
3967 [Ne III],H7	27.8	22.7	24.8	24.9	27.6	24.0	42.9	6.92	5.45	19.2	38.6	6.90
3970 H7	6.86	16.0	12.3	14.0	12.9	17.7	15.2	10.9	16.3	13.0	21.5	18.7
4026 He I	2.08	3.07	1.81	2.73	1.95	2.72	3.03	1.80	5.33	1.95	3.09	3.24
4068 [S II]	1.16	2.39	1.69	4.19			5.99			1.66	2.50	2.86
4076 [S II]		2.39	0.49	1.31			1.79		2.63		0.77	
4097 N III	0.50	4.35		1.29	3.49		1.80		5.90		0.80	0.65
4101 Hδ	24.6	26.0	23.8	27.1	26.0	34.3	27.6	27.5	29.2	26.2	30.4	29.6
4267 C II	0.45	2.47		0.65	0.90		0.40				0.79	0.57
4340 Hγ	46.9	46.9	40.3	46.9	46.9	55.3	48.2	47.4	52.1	46.9	46.9	46.9
4363 [O III]	16.1	5.81	10.2	2.96	12.6	10.2	9.97	0.60	1.96	4.22	6.19	1.74
4471 He I			3.64		11.3	10.3	4.94	8.69	6.33			
4645 N III,C III							3.47					
4658 C IV			1.63									
4686 He II				29.1		7.49						
4861 Hβ			100		100	100	100	100	100			
4959 [O III]			257		425	379	605	138	177			
5007 [O III]			883					456	499			

	M 2-23	M 2-30	M 3-20	M 3-21	M 3-7	M 3-8		M 2-23	M 2-30	M 3-20	M 3-21	M 3-7	M 3-8
5517 [Cl III]		7.74					6584 [N II]	12.7	18.4		64.3	40.6	102
5755 [N II]	1.20			3.34			6678 He I	3.42			4.85	3.33	3.65
5876 He I	12.7	11.1	13.7	21.2	13.8	16.7	6717 [S II]					2.77	4.70
6300 [O I]	1.85						6725 [S II]	1.49			9.94		
6363 [O I]	1.95						6731 [S II]					1.08	5.61
6435 [Ar V]					3.00		7065 He I	6.67		4.16	9.48	2.97	6.96

Table 4 – *continued*

6563 Hα	285	334	285	285	285	285	7325 [O II]	12.6	21.0	2.97	5.75

	AAT 1978 PNe					
	Ae 1-1	**H 1-63**	**Hubble 8**	**He 2-436**	**IC 4673**	**PC 14**
c(Hβ)	0.59	0.65	0.77	0.95	1.66	0.87
3426 [Ne V]	254				31.9	
3727 [O II]	16.6	37.0	16.2	6.68	24.1	53.5
3726/3729			2.01	2.67		
3750 H12			1.84	2.00		1.89
3760 O III						0.64
3770 H11	6.99	2.56	2.37	2.95		3.02
3798 H10	4.90	4.5	3.45	4.17		4.57
3820 He I			0.91	0.97		2.15
3835 H9	11.0	6.24	5.72	6.88		6.74
3868 [Ne III]	65.2	19.9	55.5	60.0	130	106
3889 He I,H8	10.8	12.6	16.5	18.3		17.3
3967 [Ne III],H7					39.8	
4026 He I	5.76	2.13	1.56	2.03		2.11
4068 [S II]			2.10			2.36
4072 [S II]	10.3			3.73		
4076 [S II]			0.62	27.8		1.05
4097 N III						
4101 Hδ	30.0	27.4	25.8	46.9	30.8	26.6
4267 C II						0.65
4340 Hγ	46.9	46.8	46.9		47.0	46.9
4363 [O III]	21.8	2.57	12.2		14.3	3.96
4471 He I		3.77	6.41	4.72		4.57
4686 He II	110		1.08	0.91	92.9	
4740 [Ar IV]	6.38		2.62		8.31	
4861 Hβ	100	100	100	100	100	100
4959 [O III]	149	144	449	305	417	495
5007 [O III]	490		1359	1046		1592
5517[Cl III]			0.44			
5537{[Cl III]			0.60			
5755 [N II]		2.21	0.57			
5876 He I	4.07	12.2	21.2	15.1	7.66	15.2
6300 [O I]			4.38	4.11		2.44
6312 [S III]		0.9:	1.82	0.90	2.25	
6363 [O I]			1.27	1.28		1.30
6548 [N II]		11:		4:	10.2	11.5
6563 Hα	285	285	285	285	285	285
6584 [N II]	6.27	29.4	22.8	6.13	24.7	34.7
6678 He I		1.96	3:	2:	2:	3:
6717 [S II]			0.76		3.33	3.10
6731 [S II]			1.43		2.67	4.95
7065 He I		4.68	7.79	8.16	1.75	2.41
7135 [Ar III]	5.98	9.68	12.1	3.91	20.5	9.30
7325 [O II]		35.4	7.30	6.94	4.91	2:

* Ratag (1990), + Price (1991), ! an unusually high flux, resulting in the T_e and n_e diagnostic curves not crossing, which thus cannot be deduced. & Aller & Keyes (1987), # Webster (1988), a not bulge PN, $ see Middlemass entry, (**a,b**) from fields F456, F455, @ This flux is very different to that from the two FLAIR spectra, which are 45 and 66 (the former being chosen). The line is not recorded by Acker et al. (1991), so we consider it to be uncertain, although find no fault with our spectra.

value of c(Hβ) determined from a comparison of the radio and Hβ fluxes produces a more accurate value of the reddening than the Balmer decrement method, as used here. In Fig. 1 are plotted the c(Hβ) values for our PNe against their radio c(Hβ) values, taken from Middlemass (1990) and Cahn, Kaler & Stanghellini (1992). In common with many other such comparisons, the Balmer line c(Hβ) values are systematically larger than the radio c(Hβ) values (e.g. Cahn et al. 1992). This is consistent with the finding that the value of R_V towards the bulge PNe is lower ($R_V = 2.3$) than the standard Galactic value of 3.1 (see Walton, Barlow & Clegg 1993; Liu et al. 2001). We have not attempted to deredden our spectra using $R_V = 2.3$, and so the absolute values of c(Hβ) may therefore not be correct; our goal here is merely to obtain the correct dereddened Balmer line relative intensities.

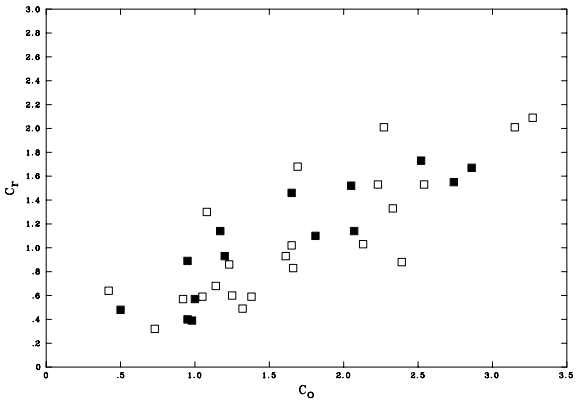

Figure 1. $c(\mathrm{H}\beta)$ extinction values calculated from the radio/Hβ ratio, c_r, versus those derived from the optical Hα/Hβ ratio, c_o, for our bulge PNe. Filled symbols are for those PNe for which abundances were later determined, empty symbols are for those without abundance determinations.

3 NEBULAR ANALYSIS

3.1 Electron temperatures and densities

Nebular electron temperatures and densities (T_e and n_e) were obtained from some or all the following forbidden line ratios:

$T_{e(\mathrm{O\,III})}$: $(I(4959) + I(5007))/I(4363)$,

$T_{e(\mathrm{N\,II})}$: $(I(6548) + I(6584))/I(5755)$,

$n_{e(\mathrm{S\,II})}$: $I(6717)/I(6731)$,

$n_{e(\mathrm{O\,II})}$: $I(3726)/I(3729)$,

where I is the dereddened flux ratioed to that of Hβ (henceforth 'line fluxes' mean these ratios). For two PNe, n_e(O II) was obtained from the ratio I(3727)/I(7325),[2] as the I(3726)/I(3729) ratios were not available. The large wavelength difference between 3727 Å and 7325 Å brings in a significant dependence on the accuracy of the relative spectral calibration, hence it is not the preferred ratio for density determinations. If both T_e(O III) and T_e(N II) could be calculated, the former was adopted for the doubly and higher ionized species and the latter for the singly ionized species; the [O III] lines generally have higher measurement accuracy (they are close to Hβ and are of good S/N) and O^{2+} is usually a more dominant ion over more of the nebula than N^+. High values of T_e(N II) (>15 000 K) were checked against the [N II] line fluxes; such nebulae are usually of Type I, associated with high [N II] line fluxes. If in doubt, we favoured the T(O III) value. Published line ratios were very occasionally used to calculate the T_e or n_e ratios, if the appropriate lines could not be measured on our spectra.

The programmes EQUIBand RATIO(I.D. Howarth and S. Adams) were used to solve the equations of statistical equilibrium in order to obtain n_e and T_e values, which are then found from the point on a plot of n_e versus T_e where the respective curves cross. In the calculation of T_e using [N II] 5755 Å, account for the contribution owing to recombination was not made. If we adopt the corrections given by Liu et al. (2000) and Tsamis et al. (2003) then for a large subsample of the bulge (and KB94 disc) PNe we find that the 5755-Å fluxes are altered by < 1 per cent: these corrections are only necessary in special cases of very high heavy element abundances or when almost all the elemental abundance is in the ion that is recombining. The atomic data used for the diagnostic and abundance analyses are referenced in Table 5, and the derived values of T_e and n_e are listed in Table 6, where the use of any published data is appropriately noted.

[2] 3727 Å=3726 + 3729 Å, 7325 Å= 7319 + 7320 + 7330 + 7331 Å

Table 5. References for atomic data.

Ion	Transition Probabilities	Collision strengths
O^+	Zeippen (1982)	Pradhan (1976)
O^{2+}	Nussbaumer & Storey (1981)	Aggarwal (1983)
N^+	Nussbaumer & Rusca (1979)	Stafford et al. (1994)
Ar^{2+}	Mendoza & Zeippen (1983)	Johnson & Kingston (1990)
Ar^{3+}	Mendoza & Zeippen (1982a)	Zeippen, Butler & Le Bourlot (1987)
Ar^{4+}	Mendoza & Zeippen (1982b)	Mendoza (1983)
Ne^{2+}	Mendoza (1983)	Butler & Zeippen (1994)
S^+	Mendoza & Zeippen (1982a) Keenan et al. (1993)	Keenan et al. (1996)
S^{2+}	Mendoza & Zeippen (1982b)	Mendoza (1983)

For some PNe it was not possible to calculate a value of T_e because the [O III] 4363 Å or [N II] 5755 Å lines were not detected. For those PNe for which the S/N in these wavelength regions is good (i.e. the lines were not detected because of faintness) we have calculated an upper limit to the flux of [O III] 4363 Å, and thus to T_e(O III), based on the value of the continuum flux in the 4363 Å region and the estimated percentage of I(4340) that would have been detected. These upper limit T_e values and the derived n_e values are given in Table 7. There is no trend for these PNe to have particularly high or low T_e.

The distributions of T_e and n_e for our bulge PNe and the KB94 disc PNe are slightly different (Fig. 2). Although the n_e distributions of the bulge and disc PNe compare fairly well to each other, there are more at the lower values in the disc, consistent with nebulae of lower density and surface brightness being easier to detect outside the bulge. The T_e(O III) distribution for the bulge PNe is displaced to lower values (mean ∼8000 K) compared with that of the disc PNe (mean ∼12 000 K). Preempting later discussion, this is also consistent with the fact that far more disc PNe have He^{2+} recombination lines present than do the bulge PNe, i.e. we find a higher proportion of high excitation class PNe in the disc sample than our FLAIR II bulge sample, following the Webster (1988) excitation class criteria: although, when classifying with the Aller (1956) excitation class criteria, this is not nearly as obvious. Higher excitation nebulae, with hotter central stars, will be on average older and are therefore expected to be larger and fainter. In the crowded fields of the bulge such lower surface brightness nebulae will be selected against. The Middlemass bulge PNe were selected to be of low excitation as their study required the central star spectrum to be seen. This affects the T_e distribution of Fig. 2 – including only the FLAIR II PN shifts the weight of the distribution to higher values – but for the n_e distribution the two peaks are not changed (if anything, the wider peak is made narrower).

We find errors of ±15 per cent on T_e values and (possibly pessimistic) ± 0.3 dex on n_e values. These were calculated by looking at the average deviation on the T_e–n_e plots caused by the propagated errors. Systematic errors will additionally be incurred, as the nebulae are unlikely to all have homogeneous temperature and density distributions. The magnitude of the effect cannot easily be

Table 6. Bulge PN electron temperatures and densities. Values in *italic* text were not adopted. Values from the literature are: A Ratag (1990); B Webster (1988); C Middlemass (1990); D Adams (1982); E Aller & Keyes (1987); F De Marco (1997); De Marco et al. (2001); G Acker et al. (1991); H Kingsburgh & English (1992); I Price (1981). A ':' result is uncertain. Densities listed without a temperature were calculated at $T_e = 11\,600$ K.

	T_e(O III)	T_e(N II)	n_e(S II)	n_e(O II)$^d_{na}$	n_e(O II)^e_n		T_e(O III)	T_e(N II)	n_e(S II)	n_e(O II)$_{na}$	n_e(O II)$_n$		T_e(O III)	T_e(N II)	n_e(S II)	n_e(O II)$_n$
	10^3 (K)			log (cm^{-3})			10^3 (K)			log (cm^{-3})			10^3 (K)		log (cm^{-3})	
	FLAIR PNe					M 3-44			3.5			H 1-42				3.7
Al 2-H			1.9:			M 3-48		7.9	2.8			H 1-53	8.7	12.7	*3.80*	4.26
Al 2-I			3.2			M 3-51	*12.5*	9.2	2.5			H 1-54	9.4	13.2	*2.97*	3.65
Al 2-Q			2.9			NGC 6565	10.6	9.6	3.2	*3.7*		H 1-55		6.8	*3.43*	3.65
Bl Q		12.3	3.5			Pe 1-12	15.5		3.5			H 1-60	9.2			3.72
H 1-17	13.9	*15.6*	4.1	*3.86*		ShWi 2-1			2.7			H 1-63	10.0	*13.8*		4.69
H 1-19		11.5	3.4			Th 3-16			3.0	*3.3*		H 4-1			2.9	
H 1-23		9.1::	3.5			Th 3-19	13.4		3.5[b]			He 2-112				3.4
H 1-44		9.2	3.5	*2.8*		H 3-26			3.3			IC 4673				2.9
H 1-46	10.3:	14.4	3.6			*Using some data taken from the literature*						KFL 01				2.7
	9.9	*11.2*		*4.5*		Al 2-E	17.1A		3.1			KFL 03				2.5
H 1-47		5.2	3.8			Ap 1-12		9.0A	3.8			KFL 16				3.1
H 1-50	11.4	*13.8*	3.5	*4.0*		H 1-18		10.0	3.9E			M 1-25	8.8		*3.91*	3.72
H 1-54	8.8	11.0	4.2	*4.7*		H 1-20	8.0B	8.8B	3.4			M 1-27			3.8	3.5
H 1-56	7.6		3.2	*4.0*		H 1-40	*15.4:*		3.1[a]	4.3		M 1-29	10.0	12.0		3.52
H 1-62		5.8	3.8				9.1A	*11.6A*				M 1-30	9.6	9.2	*3.20*	3.54
H 2-10			3.3			H 1-55	5.3I		*3.5*		3.4D	M 1-35	8.0	*14.7*	*3.21*	3.31
H 2-13			3.5			H 2-32		*21.3::*	3.8::			M 1-38		7.9	*3.74*	3.67
H 2-31		8.7::	3.6					26.5A	3.9A			M 1-42				3.1
H 2-33			3.2			H 2-39	13.3		*2.0*			M 2-11				3.4
H 2-40		8.8	2.2						3.2A			M 2-16				3.6
H 2-41	11.5	*15.1*	2.9	*3.8*		M 1-26	9.3D	9.1D	4.0[a]	4.8D		M 2-20	7.6:	*9.0:*		3.63
Hubble 5	13.3	10.3	3.5		*3.61H*			*10.7*				M 2-21				3.8
IC 4673	11.2	*9.7:*	3.2			M 1-27	10.0C		3.6	*3.1*	*3.5C*	M 2-22				3.3
K 1-4		8.4::	2.3			M 1-44		6.6B	3.2			M 2-23	12.8	*>19.0*		3.74
KFL-01			*4.1*		2.71C	M 2-20		*6.6*	*3.5*	*4.2*		M 2-27				3.6
KFL-03	15.2:		2.4					7.35C	3.6			M 2-29	20.6			3.46
KFL-05	26.0:	26.0	3.5[b]			M 2-27	7.9 A	*10.3A*	*3.7*			M 2-30	11.4			3.47
KFL-09	17.8		3.1:				*8.8:*	9.2				M 3-7	6.8:			3.63
M 1-29	10.0	8.4	3.6			M 2-29	19.4		*3.5*	*2.7*	3.2D	M 3-8	8.6		*3.00*	3.09
M 1-37		5.9	3.8			M 2-33	8.4E		3.1			M 3-20	11.1			3.97
M 1-42	9.2	8.6	*3.0*	*3.7*	3.0	M 3-23	12.8 G		3.1			M 3-21	9.5	*17.9*	2.76	3.82
M 2-19		7.5	2.9			M 3-42	10.4B	8.0	3.0			M 4-3				4.0
M 2-23	11.7	*19.3*	*4.0*	*4.8*	3.7	M 3-45	13.7B:		3.3			PC 14				3.4
M 2-25		8.3	2.6			M 4-6		*15.5::*	*3.7*			Vy 2-1				3.6
M 2-26		7.8	2.9					*14.5A*	*3.8A*					AAT 1978 PNe		
M 2-28	*10.2:*	8.0	3.2					12.6B	4.3B			Hubble 8	11.0	*13.9*	*3.8*	3.7
M 2-30	10.5		3.3[a]	3.9		SwSt 1	10.5F	10.5F			4.5F	IC 4673	12.5		*2.3:*	
M 2-32	12.2		3.2				*12.1*	*10.0*	*4.0*		*5.3*				3.2[c]	
M 2-36	8.2	9.6	3.5	*4.5*				Middlemass PNe				He 2-436	9.9		4.4	
M 3-16[x,y]			3.0			Cn 1-5	8.9	8.5			3.64	PC 14	7.8	3.4		
M 3-22	16.1		3.0			H 1-20			3.87			Ae 1-1	24.4	3.0[b]		
M 3-26	10.7	*18.5*	3.3	*4.3*		H 1-35	9.1	*14.6*			4.26					

a: Used when deriving A(S^+). *b* assumed value. *c* from FLAIR spectrum. *x*: F455. *y*: F456. *d*: nebular/auroral: 3727/7325. *e*: nebular: 3726/3729

Table 7. Limits to T_e and abundances [as log(X/H)+12.0 except for He/H], for PNe with an upper limit to the flux ratio $I(4363)/I(H\beta)$. The Webster (1988) excitation class is also given.

	H 2–10	H 2–13	M 3–16a	M 3–16b	M 3–19	Th 3–26	H 1–20
$I(4363)$	<9	<29	<10	<5	<6	<17	<10
$\frac{I(5007+4959)}{I(4363)}$	>155	>72	>92	>188	>112	>102	>31
T_e (K)	<9550	<14300	<12600	<8800	<11300	<11800	<22100
log n_e (cm^{-3})	3.2	3.6	3.0	2.6	2.9	3.2	4.5
	O/H	Ne/H	S/H	Ar/H	N/H	He/H	Ex.Cl.
H 2-10	>8.74	–	>6.48	>6.20	>7.24	>0.091	2
H 2-13	>8.32	–	>6.36	>6.20	>7.80	>0.086	2
M 3-16^{F456}	>8.14	>7.24	>6.26	>6.03	>7.51	>0.097	3
M 3-16^{F455}	>8.74	>8.16	>6.67	>6.39	>7.65	>0.093	3
M 3-19	>8.18	>7.60	–	>6.26	>7.01	>0.129	3
Th 3-26	>8.62	–	>6.82	>6.54	>8.29	>0.136	9
H 1-20	>7.75	>6.89	>6.15	>5.89	>8.62	>0.074	4

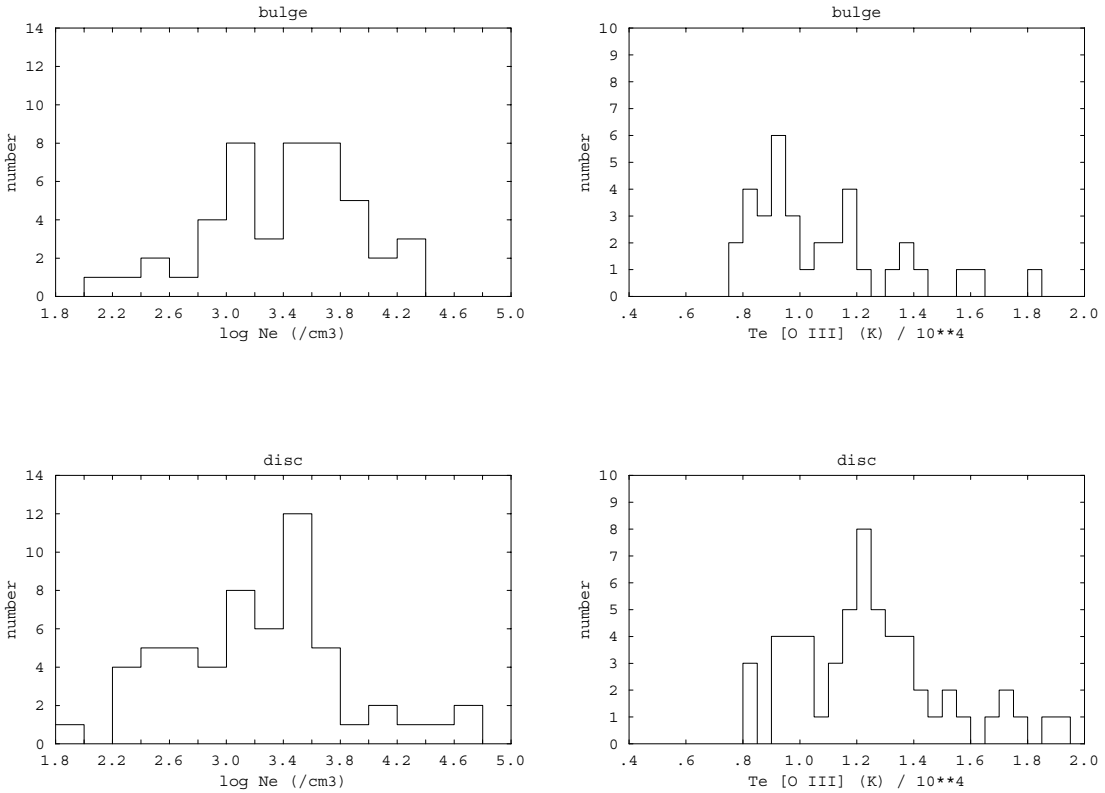

Figure 2. The distribution of adopted T_e(O III) and log n_e (S IIor O II) for our bulge PNe (top) and the KB94 disc PNe (bottom).

estimated for individual bulge PNe, but we do discuss the matter again later.

3.2 Abundance calculations

3.2.1 Helium

He II 4686 Å is produced by radiative recombination, while the He I 4471, 5876, 6678, 7065 Å lines are produced predominantly by radiative recombination, with an additional contribution from collisional excitation from the 2^3S metastable level of He^0. Collisions affect the 7065-Å flux the most; this line was never used to obtain a He^+ abundance. For the other three He I lines, we employed the collisional correction formulation of Kingdon & Ferland (1995), via a programme written by X.-W Liu. The later corrections of Benjamin, Skillman & Smits (2002) were compared with ours, and for the density regime in which these later values are valid (as stated by the authors), log n_e < 2.3 (in fact, we tested up to 3.4), the derived He^+/H^+ abundances agree to better than ±10 per cent. Helium ionic abundances were derived assuming Case B recombination (taken from Osterbrock 1989, which were taken from Brocklehurst 1971, for H I; Brocklehurst 1972 for He I; Hummer & Storey 1987, for He II). The final He^+ abundances relative to H^+ are a weighted mean of the individual values from 6678, 5876 and 4471 Å for the 'AAT 1978' and Middlemass PNe (4471 Å was of low S/N on the FLAIR II spectra). The weights adopted were based on the quality of the measured fluxes. The sum of the He^+ and He^{2+} abundances[3] gives the total He abundance. The derived helium abundances are listed in Table 8 for each nebula.

[3] Henceforth 'A(He^+)', or 'the He^+ abundance' means the abundance ratio He^+/H^+; likewise for other ions or elements.

Table 8. The nebular abundances for the PNe included in the abundance analysis. Webster excitation classes, and the KB94 Type I (I) or non-Type I (nI) are also indicated. Column 4, 6, 8, .. are the relative weights (no weight = 0) or quality comments; 'ul' upper limit (adopted only if no other value available), ':,::' uncertain value, 'p' present but not measured, () are assumed values. Abundances derived from FLAIR II spectra unless otherwise stated. Some PNe lack a value for $A(O^+)$, hence the ICF for other elements could not be calculated.

		Ae 1-1$^+$		**Bl-Q**		**Cn 1-5***		**H 1-17**		**H 1-18**		**H1-20**		**H 1-23**		**H 1-35***		**H 1-40**	
4471	He^+/H^+					0.149	1									0.108	1		
5876	He^+/H^+	0.0233	:	0.0893	1	0.196		0.0781	1	0.0920	1	0.0994		0.105	1	0.101	3	0.0899	1
6678	He^+/H^+			0.114	1	0.133	3	0.0941	1	0.160	2	0.124	3	0.120	1	0.062		0.112	1
4686	He^{2+}/H^+	0.103	1																
	He/H	0.103		0.102		0.137		0.086		0.137		0.112		0.113		0.103		0.101	
3727	$10^5\times O^+/H^+$	0.049	1			17.9	1	3.41	:							12.2		7.31	
7325	$10^5\times O^+/H^+$			1.54	ul	12.6	1	2.18	2	7.47	1	16.8	1	10.3	1	29.0	1	14.9	1
4363	$10^4\times O^{2+}/H^+$	0.20	1			4.43	1	2.02				8.04	1			2.73		21.7	ul
4959	$10^4\times O^{2+}/H^+$	0.18	1	2.06	1	4.50	1	1.97	1	4.82	1			5.92	1	2.71	1	5.19	1
5007	$10^4\times O^{2+}/H^+$	0.20	1	1.87	1	5.65		2.02	1	5.23	1			6.26	1	3.06	1	5.06	1
	ICF(O)	*5.89*		*1.00*		*1.00*		*1.00*		*1.00*		*1.00*		*1.00*		*1.00*		*1.00*	
	$10^4\times O/H$	1.15		2.12		5.99		2.26		5.77		9.38		7.12		5.79		12.2	
5755	$10^5\times N^+/H^+$			1.16		7.77	1	0.76		4.20		4.05	1	1.82	::	3.27			
6548	$10^5\times N^+/H^+$			1.08	1	8.40	1	0.59	1	4.41	1	4.67	1	1.70	1	1.16	1	1.31	1
6584	$10^5\times N^+/H^+$	2.06	1	1.19	1	6.95	:	0.64	1	4.18	1			1.86	1	1.21	1	1.45	1
	ICF(N)	*39.7*		*13.7*		*3.93*		*8.72*		*7.73*		*5.86*		*6.94*		*1.99*		*8.14*	
	$10^4\times N/H$	8.17		1.56		3.18		0.54		3.32		2.56		1.24		2.37		11.2	
3868	$10^5\times Ne^{2+}/H^+$	0.52	1			13.3	1	7.03	:			23.8	1			3.38	1		
3967	$10^5\times Ne^{2+}/H^+$															3.69	1	12.1	ul
4012	$10^5\times Ne^{2+}/H^+$					13.2	1					0.72	1						
3426	$10^5\times Ne^{4+}/H^+$	1.54	1																
	ICF(Ne)	*1.5*				*1.34*		*1.13*				*1.21*				*2.01*		*1.14*	
	$10^5\times Ne/H$	3.09				17.8		7.95				28.6				7.08		13.7	
7135	$10^6\times Ar^{2+}/H^+$	1.14	1	1.25	1	2.96	1	1.16	1	2.96	1	4.83	1	2.73	1	1.01	1	2.09	1
4740	$10^7\times Ar^{3+}/H^+$	2.19	1																
7005	$10^7\times Ar^{4+}/H^+$																		
	ICF(Ar)	*1.03*		*1.87*		*1.87*		*1.87*		*1.87*		*1.87*		*1.87*		*1.87*		*1.87*	
	$10^6\times Ar/H$	1.40		2.34		5.53		2.17		5.54		9.02		5.10		1.88		3.91	
4068	$10^7\times S^+/H^+$					19.3	1									4.51	1		
6717	$10^7\times S^+/H^+$			4.31	1	17.2	1	2.38	1	10.2	1	10.1	1	5.65	1			2.21	ul
6725	$10^7\times S^+/H^+$															1.94	:		
6731	$10^7\times S^+/H^+$			4.48	1	14.3	1	2.47	1	12.5	1	10.4	1	5.87	1			2.18	ul
6312	$10^6\times S^{2+}/H^+$			(3.38)	1	(10.6)	1	1.98	1	6.76	1	9.28	1	5.82	1	(2.59)	1	(1.54)	1
	ICF(S)			*1.70*		*1.20*		*1.48*		*1.43*		*1.33*		*1.39*		*1.05*		*1.45*	
	$10^6\times S/H$			6.49		1.48		3.30		11.3		13.7		8.89		3.19		2.55	
Ex. cl., KB Type		9,I		2,nI		4,nI		4,nI		2,nI		4,nI		2,nI		2,nI		4,nI	

		H 1-44		**H 1-46**		**H 1-50**		**H 1-53***		**H 1-54***		**H 1-56**		**H 1-60***		**H 2-39**		**H 2-40**	
4471	He^+/H^+			0.108				0.171		0.0588		0.0906		0.237					
5876	He^+/H^+	0.0980	1	0.0957	1	0.0827	1	0.109	2	0.0929	1	0.0854	1	0.0945	1	0.0606	1	0.0923	1
6678	He^+/H^+	0.0838	1	0.0880	1	0.118	2	0.0876	1	0.0861	1	0.0989	1	0.120		0.0698	1	0.0870	1
4686	He^{2+}/H^+					0.0093	1							0.0032	1	0.0322	1		
	He/H	0.091		0.092		0.115		0.102		0.090		0.092		0.098		0.097		0.090	
3727	$10^5\times O^+/H^+$	36.2		1.06	:	1.51	1	0.76		5.45		4.60	1	0.90	1			9.45	1
7325	$10^5\times O^+/H^+$	36.3	1	3.77	1	3.72	1	1.47	1	28.9	1								
4363	$10^4\times O^{2+}/H^+$			1.65		4.09		4.67		1.84		6.21		3.3	1	1.95			
4959	$10^4\times O^{2+}/H^+$	1.84	1	1.54	1	3.82	1	4.77	1	1.82	1	5.66	1	3.38	1	1.91	1	3.11	1
5007	$10^4\times O^{2+}/H^+$	1.82	1	1.64	1	4.13	1	5.01	1	1.86	1	6.05	1			1.95	1	3.20	1
	ICF(O)	*1.00*		*1.00*		*1.06*		*1.00*		*1.00*		*1.00*		*1.02*		*1.31*		*1.00*	
	$10^4\times O/H$	5.46		1.99		4.48		5.03		4.74		6.32		3.55		2.52		4.10	
5755	$10^5\times N^+/H^+$	18.1		0.13	1	1.17		2.26		2.30	:							12.7	
6548	$10^5\times N^+/H^+$	17.7	1	0.33	1	0.79	1	2.02	1	1.42	1	0.48	1					11.9	1
6584	$10^5\times N^+/H^+$	18.4	1	0.36	1	0.98	1	2.54	1	1.09	1	0.51	1			0.064	1	12.9	1
	ICF(N)	*1.51*		*5.26*		*17.1*		*34.3*		*1.64*		*13.7*						*4.34*	
	$10^4\times N/H$	2.71		0.18		1.38		71.3		0.21		0.68						5.38	
3868	$10^5\times Ne^{2+}/H^+$							14.0	1	1.67	1	13.5	1	8.62	1			12.0	1
3967	$10^5\times Ne^{2+}/H^+$			2.03	1	10.2	1	2.79	1	1.88	1			6.83	1				
4012	$10^5\times Ne^{2+}/H^+$																		

Table 8 – *continued*

	ICF(Ne)		*1.23*		*1.13*		*1.03*		*2.57*		*1.08*		*1.05*				*1.30*		
	$10^5\times$Ne/H		2.50		11.5		8.65		4.56		14.6		8.11				15.5		
7135	$10^6\times Ar^{2+}/H^+$	2.48	1	0.80	1	1.06	1	3.15	1	0.72	1	2.59	1	1.38	1	0.25	1	3.05	1
4740	$10^7\times Ar^{3+}/H^+$					9.48	1									4.70	:		
7005	$10^7\times Ar^{4+}/H^+$																		
	ICF(Ar)	*1.87*		*1.87*		*1.06*		*1.87*		*1.87*		*1.87*		*1.87*				*1.87*	
	$10^6\times$Ar/H	4.64		1.49		2.14		5.90		1.36		4.84		2.58				5.70	
4068	$10^7\times S^+/H^+$							5.22		4.45	2			3.38	1				
6717	$10^7\times S^+/H^+$	22.8	1	5.98	1	3.91	1	2.64	1			1.66	1			0.64	1	37.8	1
6725	$10^7\times S^+/H^+$									1.69	:								
6731	$10^7\times S^+/H^+$	23.5	1	0.64	1	4.02	1	2.39	1			1.72	1			0.38	2	37.5	1
6312	$10^6\times S^{2+}/H^+$	(12.5)	1	3.06	:	3.03	1	(2.31)	1	6.13	:	4.07	:	(3.21)	1			(23.9)	
	ICF(S)	*1.01*		*1.29*		*1.82*		*2.28*		*1.02*		*1.70*		*2.38*				*1.22*	
	$10^6\times$S/H	15.0		4.02		6.24		5.84		6.61		7.22		8.44				33.7	
	Ex. Cl., KB Type	0.5,nI		2,nI		5,nI		4,I		1,nI		3,nI		5,nI		7.5,nI		4,I	

		H 2-41		**He 2-436**[a+]		**Hubble 5**[b]		**Hubble 8**$^+$		**IC 4673**[b]		**K 1-4**[b]		**KFL-09**		**M 1-25**[*]		**M 1-29**[b]	
4471	He^+/H^+	0.130		0.0930	1	0.0693		0.123	1	0.119						0.116	1	0.0958	
5876	He^+/H^+	0.0963	1	0.103	3	0.0714	1	0.137	3	0.0675	1	0.0933	1	0.0224	1	0.116	2	0.100	1
6678	He^+/H^+	0.157	2	0.0585		0.107	2	0.0812		0.0888	1			0.0433	2	0.0945	1	0.114	1
4686	He^{2+}/H^+	0.0265	1	0.00072	1	0.0457	1	0.00087	1	0.0540	1			0.0947	1		1	0.0295	1
	He/H	0.164		0.101		0.141		0.134		0.132		0.093		0.131		0.111		0.137	
3727	$10^5\times O^+/H^+$	7.93		1.20		3.60	1	0.697	1	0.878	1					12.4	1	10.2	2
7325	$10^5\times O^+/H^+$	2.23	1	4.00	1	29.7		3.51		1.31	1					13.0	1	32.5	1
4363	$10^4\times O^{2+}/H^+$	1.05	1	7.01		2.59		3.62	1	2.85	1			0.47		2.68		5.10	
4959	$10^4\times O^{2+}/H^+$	1.08	1	3.39	1	2.61	1	3.43	1	2.79	1	5.98	1	0.45	1	2.63	1	5.05	1
5007	$10^4\times O^{2+}/H^+$	1.08	1	4.03	1	2.61	1	3.61	1	2.71	1	6.37	1	0.47	1	3.12	1	4.83	1
	ICF(O)	*1.12*		*1.00*		*1.30*		*1.00*		*1.42*		*1.00*		*2.35*		*1.00*		*1.18*	
	$10^4\times$O/H	1.45		4.13		3.86		3.64		4.10		6.18		1.08		4.15		7.88	
5755	$10^5\times N^+/H^+$	0.45	1			11.5		0.38	1			14.4						8.75	
6548	$10^5\times N^+/H^+$	0.49	1	0.24	:	11.1	1	0.34	1	0.44	1	13.2	1			5.12	1	9.04	1
6584	$10^5\times N^+/H^+$	0.76		0.14	1	11.9	1	0.32	1	0.48	1	14.6	1	0.02	1	5.55	1	9.51	1
	ICF(N)	*6.56*		*10.3*		*10.7*		*52.2*		*37.6*						*3.26*		*4.48*	
	$10^4\times$N/H	0.31		0.15		12.3		1.81		1.74						1.74		4.15	
3868	$10^5\times Ne^{2+}/H^+$	3.07	1	6.25	1	2.77	1									1.12	1		
3967	$10^5\times Ne^{2+}/H^+$							3.84	1	8.05	1			0.861	1	1.17	1	11.6	1
4012	$10^5\times Ne^{2+}/H^+$																		
3426	$10^5\times Ne^{4+}/H^+$																		
	ICF(Ne)	*1.35*		*1.11*		*1.48*		*1.02*		*1.48*				*2.35*		*1.44*		*1.60*	
	$10^5\times$Ne/H	4.16		6.95		4.09		3.94		11.9				2.02		1.65		18.6	
7135	$10^6\times Ar^{2+}/H^+$	0.84	1	0.33	1	3.17	1	0.81	1	2.57	1	2.21	1	0.18	1	2.12	1	4.06	1
4740	$10^7\times Ar^{3+}/H^+$					11.9	1	3.55	1	8.31	1							8.87	1
7005	$10^7\times Ar^{4+}/H^+$					6.70	1			2.32	1							2.88	1
	ICF(Ar)	*1.87*		*1.87*		*1.10*		*1.02*		*1.03*		*1.87*		*1.87*		*1.87*		*1.29*	
	$10^6\times$Ar/H	1.61		0.62		5.55		1.19		3.74		4.13		0.35		3.97		6.74	
4068	$10^7\times S^+/H^+$							2.90								14.0			
6717	$10^7\times S^+/H^+$	p				17.0	1	0.67	1	3.19	1	32.4	1	0.17	:	7.14	1	31.1	1
6731	$10^7\times S^+/H^+$	p				17.5	1	0.75	1	3.27	1	32.5	1	0.17	:	7.92	1	35.	1
6312	$10^6\times S^{2+}/H^+$	p		1.93	1	2.64	1	2.73	1	3.71	1					7.06	1	7.62	1
	ICF(S)			*1.56*		*1.58*		*2.61*		*2.34*						*1.14*		*1.23*	
	$10^6\times$S/H			3.02		6.88		7.32		9.45						8.94		13.3	
	Ex. cl., KB Type	7.5,nI		4,nI		7.5,I }		4,nI		9,nI		2,nI		9,nI		5,nI		7.5,nI	

		M 1-35[*]		**M 1-42**		**M 2-19**		**M 2-20**[*]		**M 2-23**		**M 2-25**		**M 2-26**		**M 2-27**		**M 2-28**	
4471	He^+/H^+	0.243		0.140	1			0.125	1	0.0958	1	0.0715				0.0894		0.109	1
5876	He^+/H^+	0.156	1	0.126	1	0.0790	1	0.00932	3	0.100	2	0.0974	1	0.101	1	0.101	1	0.119	1
6678	He^+/H^+	0.176	1	0.159	1	0.0946	2	0.0822		0.0695	1	0.0897	1	0.105	1	0.130	1	0.124	1
4686	He^{2+}/H^+			0.0094	1	0.0109	1					0.0179	1	0.0155	1	0.0014	1	0.0127	1
	He/H	0.166		0.151		0.100		0.101		0.091		0.111		0.119		0.116		0.130	
3727	$10^5\times O^+/H^+$	6.17	1	52.2	1	40.1	1	11.7	1	6.37	1	78.7				5.03	1	20.8	1
7325	$10^5\times O^+/H^+$			14.8		36.5	1	8.64		0.567		17.6	1			6.53	1	20.6	1
4363	$10^4\times O^{2+}/H^+$	6.23		2.41	1			1.48		2.30		5.19	1			1.19		13.5	
4959	$10^4\times O^{2+}/H^+$	5.85	1	2.33	1	1.72	1	2.79	1	2.41	1			5.36	1	7.11	1	5.23	1
5007	$10^4\times O^{2+}/H^+$	6.44	1	2.36	1	1.54	1			2.48	1	5.17	1	5.67	1	7.90	1	5.59	1

Table 8 – *continued*

	ICF(O)	*1.00*		*1.04*		*1.08*		*1.00*		*1.00*		*1.12*		*1.10*		*1.00*		*1.07*	
	$10^4\times$O/H	6.76		3.01		5.88		3.96		3.04		7.80		6.05		8.08		8.01	
5755	$10^5\times N^+/H^+$	19.1		6.13		6.70		2.46	1	0.21	1	11.8	1	8.32		3.18		14.3	
6548	$10^5\times N^+/H^+$	5.32	1	5.51	1	7.11	1	2.51	1	0.24	1	11.3	1	7.73	1	3.32	1	14.5	1
6584	$10^5\times N^+/H^+$	4.79	1	5.56	1	7.37	1	2.43	1	0.51		12.0		8.02	1	3.31	1	14.1	1
	ICF(N)	*11.0*		*5.77*		*1.54*		*3.39*		*4.76*		*4.43*				*14.0*		*3.87*	
	$10^4\times$N/H	5.54		3.20		1.11		0.84		0.11		5.15				4.51		5.54	
3868	$10^5\times Ne^{2+}/H^+$	18.6	1	9.39	1			1.03	:	4.90	1	1.11	1	3.72		2.23	1	23.3	1
3967	$10^5\times Ne^{2+}/H^+$	6.54	1					2.49	1										
4012	$10^5\times Ne^{2+}/H^+$																		
3426	$10^5\times Ne^{4+}/H^+$																		
	ICF(Ne)	*1.10*		*1.27*				*1.42*		*1.27*		*1.51*				*1.08*		*1.48*	
	$10^5\times$Ne/H	13.9		12.0				3.53		6.20		16.5				24.1		34.5	
7135	$10^6\times Ar^{2+}/H^+$	3.33	1	2.43	1	1.84	1	1.31	1	0.794	1	4.05	1	3.25	1	4.44	1	4.60	1
4740	$10^7\times Ar^{3+}/H^+$			3.59	1					1.07	1								
7005	$10^7\times Ar^{4+}/H^+$																		
	ICF(Ar)	*1.87*		*1.21*		*1.87*		*1.87*		*1.27*		*1.87*		*1.87*		*1.87*		*1.87*	
	$10^6\times$Ar/H	6.24		3.37		3.43		2.44		1.14		7.57		6.08		8.30		8.60	
4068	$10^7\times S^+/H^+$							13.8		60.9	1								
6717	$10^7\times S^+/H^+$	9.02	1	14.3	1	26.2	1	3.75	1	0.57	1	55.5	1	18.2	1	8.43	1	39.2	1
6731	$10^7\times S^+/H^+$	8.84	1	14.6	1	26.8	1	3.69	1			56.0	1	18.2	1	8.63	1	40.1	1
6312	$10^6\times S^{2+}/H^+$	(7.00)	1	3.91	1	6.21	ul	(2.28)		1.85	1	6.64	1			10.3	1	8.56	1
	ICF(S)	*1.59*		*1.32*		*1.01*		*1.15*		*1.25*		*1.23*				*1.71*		*1.19*	
	$10^6\times$S/H	12.5		7.06		8.99		3.05		2.39		15.0				19.0		1.49	
Ex. cl., KB Type		4,I		5,I		5,nI		2,nI		4,nI		6,nI		6,nI		4,nI		6,nI	

		M 2-29[c]		**M 2-30**[*]		**M 2-32**		**M 2-33**		**M 2-36**		**M 3-8**[*]		**M 3-20**[*]		**M 3-21**[*]		**M 3-22**	
4471	He^+/H^+	0.0969	1	0.282		0.0867		0.0842		0.1100	1	0.124	2	0.193		0.0959			
5876	He^+/H^+	0.0811	1	0.0693:	1	0.0915	1	0.0824	1	0.0994	1	0.113	3	0.0852	1	0.139	1	0.0158	
6678	He^+/H^+	0.119	1			0.105	1	0.0940	1	0.127	1	0.0869	1			0.117		0.0460	1
4686	He^{2+}/H^+		1	0.0274	1	0.0020	1			0.0019	1					0.00601	1	0.0888	1
	He/H	0.099		0.096		0.098		0.088		0.114		0.112		0.085		0.146		0.105	
3727	$10^5\times O^+/H^+$	0.23	1	0.288	1			2.92	1	31.1	1	7.38	1	1.66	1	3.03	1		
7325	$10^5\times O^+/H^+$	0.15	1					8.71		11.9		19.4				20.8		0.29	1
4363	$10^4\times O^{2+}/H^+$	0.27	1	1.88		2.24				5.43		3.21		2.88	1	7.53	1	0.75	1
4959	$10^4\times O^{2+}/H^+$	0.26	1	1.87	1	2.08	1	3.92	1	5.85	1	3.19	1	2.86	1	7.47	1	0.73	
5007	$10^4\times O^{2+}/H^+$	0.26	1			2.21	1	3.97	1	5.97	1	3.12	1					0.72	1
	ICF(O)	*1.00*		*1.25*		*1.01*		*1.00*		*1.01*		*1.00*		*1.00*		*1.03*		*3.52*	
	$10^4\times$O/H	0.28		2.37		2.17		4.24		6.29		3.89		3.03		8.02		2.70	
5755	$10^5\times N^+/H^+$	p								2.42						4.39	:		
6548	$10^5\times N^+/H^+$	0.093	1	0.32				0.31	1	2.66	1	2.98	1			1.99	1		
6584	$10^5\times N^+/H^+$	0.095	1	0.17	1	0.017	1	0.32	1	2.77	1	2.63	1			1.35	1		
	ICF(N)	*15.1*		*82.1*				*14.5*		*2.02*		*5.28*				*26.5*			
	$10^4\times$N/H	0.14		1.39				0.46		5.49		1.48				4.42			
3868	$10^5\times Ne^{2+}/H^+$	0.65	1	4.82	2	5.75	1	6.80	1	13.7	1	5.96	1	7.87	2	16.9	1	1.38	1
3967	$10^5\times Ne^{2+}/H^+$			6.13	1							3.39		5.25	1	18.7	1		
4012	$10^5\times Ne^{2+}/H^+$																		
3426	$10^5\times Ne^{4+}/H^+$																		
	ICF(Ne)	*1.07*		*1.26*		*1.01*		*1.07*		*1.06*		*1.23*		*1.06*		*1.07*		*3.66*	
	$10^5\times$Ne/H	0.70		6.62		5.83		7.31		14.6		7.35		7.41		19.1		5.06	
7135	$10^6\times Ar^{2+}/H^+$	0.32	1	1.37	1	0.41	1	1.41	1	3.99	1	1.90	1	0.34	1	1.29	1	0.21	1
4740	$10^7\times Ar^{3+}/H^+$			5.99	1	3.52	1			4.10	1					8.73	1	7.99	1
7005	$10^7\times Ar^{4+}/H^+$																	0.931	1
	ICF(Ar)	*1.87*		*1.01*				*1.87*		*1.05*		*1.87*		*1.87*		*1.04*			
	$10^6\times$Ar/H	0.60		1.99				2.64		4.62		3.55		0.64		2.25			
4068	$10^7\times S^+/H^+$															21.6	1		
6717	$10^7\times S^+/H^+$	0.35	1			0.22	1	0.81	1	10.1	1							0.40	ul
6725	$10^7\times S^+/H^+$											4.10	1						
6731	$10^7\times S^+/H^+$	0.38	1			0.23	1	0.88	1	10.6	1							0.40	ul
6312	$10^6\times S^{2+}/H^+$	0.21	1			0.67	ul	(0.66)	1	7.95	1	(2.69)				(18.8)	1	(0.35)	1
	ICF(S)	*1.75*						*1.73*		*1.92*		*1.29*				*2.09*		*3.17*	
	$10^6\times$S/H	0.44						1.29		17.3		4.00				43.9		1.23	
Ex. cl., KB Type		3,nI		6,nI		4,nI		3,nI		4,I		6,nI		4,nI		5,nI		9,nI	

Table 8 – *continued*

		M 3-23		**M 3-42**		**M 3-45**		**M 3-48**		**M 3-51**		**NGC 6565**[b]		**Pe 1-12**		**PC 14**[b+]	
4471	He^+/H^+	0.439								0.151		0.100				0.0885	1
5876	He^+/H^+	0.0298	1	0.0544	1	0.0663	1	0.0924	1	0.104	1	0.0907	1	0.0287	1	0.0998	3
6678	He^+/H^+	0.0556	2	0.0669	1	0.103	2			0.123	1	0.115	1	0.157		0.0749	
4686	He^{2+}/H^+	0.0755	1	0.0523	1	0.0268	1			0.0237	1	0.0129	1	0.0893	1		
	He/H	0.122		0.113		0.115		0.092		0.137		0.116		0.118		0.097	
3727	$10^5\times O^+/H^+$					0.90	1					34.6		0.94		10.2	
7325	$10^5\times O^+/H^+$			13.95	1					3.76		15.0	1			9.55	1
4363	$10^4\times O^{2+}/H^+$					2.43	1	5.25	1	2.81	1	2.73	1	0.61	1	14.8	1
4959	$10^4\times O^{2+}/H^+$	2.25	1	4.77	1					7.32		3.19		0.61		14.4	1
5007	$10^4\times O^{2+}/H^+$	2.37	1	4.83	1	2.24	1	5.57	1	2.70	1	3.26	1	0.59	1	13.3	1
	ICF(O)	*1.89*		*1.51*		*1.17*		*1.00*		*1.13*		*1.08*		*2.57*		*1.00*	
	$10^4\times O/H$	4.38		9.38		2.84		5.41		3.55		4.87		1.54		15.1	
5755	$10^5\times N^+/H^+$			4.44				18.3		4.51		8.78					
6548	$10^5\times N^+/H^+$	0.20	1	6.11	1	0.33	1	17.5	2	4.15	1	8.76	1	0.040		1.21	1
6584	$10^5\times N^+/H^+$	0.22	1	6.80	1	0.27	1	18.6	1	4.59	1	8.81	1	0.042	:	1.24	1
	ICF(N)			*6.72*		*31.8*				*9.43*		*3.25*				*15.9*	
	$10^4\times N/H$			4.34		0.96				4.12		2.85				1.95	
3868	$10^5\times Ne^{2+}/H^+$	4.44	1														
3967	$10^5\times Ne^{2+}/H^+$																
4012	$10^5\times Ne^{2+}/H^+$											7.58	1			33.1	1
3426	$10^5\times Ne^{4+}/H^+$																
	ICF(Ne)	*1.89*										*1.62*				*1.07*	
	$10^5\times Ne/H$	8.41										12.3				35.3	
7135	$10^6\times Ar^{2+}/H^+$	1.58	1	4.32	1	0.17	::	3.87	1	2.08	1	2.51	1	0.48	1	1.48	1
4740	$10^7\times Ar^{3+}/H^+$	11.3	1									2.14	1				
7005	$10^7\times Ar^{4+}/H^+$	5.15	1	8.96	1												
	ICF(Ar)			*1.87*		*1.87*		*1.87*		*1.87*		*1.45*		*1.87*		*1.87*	
	$10^6\times Ar/H$			8.07		0.34		7.23		3.90		3.94		0.89		2.77	
4068	$10^7\times S^+/H^+$					1.57	1	49.6	1	13.7	1	33.0	1			5.37	1
6717	$10^7\times S^+/H^+$	2.46	1	24.8	1											13.9	
6731	$10^7\times S^+/H^+$	1.89	1	25.4	1	1.53	1	49.3	1	13.7	1	32.2	1			5.08	1
6312	$10^6\times S^{2+}/H^+$			(16.0)	1	(1.36)	1			(9.72)	1	5.38	1			9.60	1
	ICF(S)			*1.38*		*2.22*				*1.22*		*1.14*				*1.78*	
	$10^6\times S/H$			25.5		3.36				16.9		9.88				18.0	
Ex. cl., KB Type		9,nI		9,nI		6,nI		2,nI		7.5,I		6,nI		9,nI		4,nI	

Incompletely ionized PNe

		Ap 1-12	**H 1-47**	**H 1-55***	**H 1-62**	**H 1-63***	**H 2-31**	**M 1-26**[b]	**M 1-27**	**M 1-37**	**M 1-38***	**M 1-44**	**SwSt-1**[b]
4471	He^+/H^+					0.0731		0.0401					0.0420
5876	He^+/H^+	0.0062	0.0052	0.0475	0.0102	0.0709	0.0157	0.0572	0.0080	0.0088	0.0075	0.0452	0.0394
6678	He^+/H^+		0.0105:		0.0146	0.105		0.0815				0.0595	0.0463
4686	He^{2+}/H^+												6.18
3727	$10^4\times O^+/H^+$	0.16	13.2	3.03	7.94	1.19		6.31	0.497	2.29	1.74	1.30	0.823
7325	$10^4\times O^+/H^+$					0.94		12.1	0.30	9.39	1.47		4.42
4363	$10^4\times O^{2+}/H^+$					1.14					4.09		0.162
4959	$10^4\times O^{2+}/H^+$			0.16		1.15		0.35					0.11
5007	$10^4\times O^{2+}/H^+$			0.18				0.37		0.04			0.12
5755	$10^5\times N^+/H^+$		35.5	12.6	23.7	1.10		5.47		26.9	5.94		3.82
6548	$10^5\times N^+/H^+$	5.37	34.7	13.7	22.9	0.79	6.47	8.73	3.15	25.8	6.04	13.3	2.92
6584	$10^5\times N^+/H^+$	5.31	35.2	12.5	22.8	0.76	6.88	8.44	3.33	27.3	5.93	13.2	3.17
3868	$10^6\times Ne^{2+}/H^+$	1.05				1.64							
3967	$10^6\times Ne^{2+}/H^+$					1.58							
7135	$10^7\times Ar^{2+}/H^+$			6.15	2.49 ul	5.01		1.43					8.92
4068	$10^6\times S^+/H^+$					0.42							
4740	$10^7\times Ar^{3+}/H^+$												0.43
6717	$10^6\times S^+/H^+$	1.35	9.97	1.94	8.59		1.40	0.49	1.12	5.57	1.56	3.28	0.32
6731	$10^6\times S^+/H^+$	1.38	10.4	1.87	8.99		1.44	0.51	1.15	5.89	1.67	3.39	0.36
6312	$10^6\times S^{2+}/H^+$				4.93 ul			6.39					5.11
Ex. cl.		0.5	0.5	0.5	0.5	5	0.5	0.5	0.5	0.5	-	0.5	4

* Abundances derived from 1988 Middlemass AAT data, + Abundances derived from 1978 AAT data [a]: extragalactic, [b]: foreground, [c]: Bulge PN but not included in our analysis.

3.2.2 Collisionally excited lines

Heavy-element ion abundances were calculated from collisionally excited line fluxes using multilevel statistical equilibrium calculations with EQUIB. Results from multiple measurements of an ion (e.g. O^+ from 3727 and 7325 Å) were averaged, with weights in proportion to the measurement errors. Generally problems only arose for $A(O^+)$; for 12 PNe the [O II] 3727 and 7325 Å fluxes gave values for the O^+ abundance differing by greater than a factor of 2. Owing to their different critical densities, these two lines respond differently to the nebular environment; the 3727 Å lines sample lower density material than do the 7325 Å lines, and the strengths of the latter are also more dependent on T_e than are the former. Based on these facts and the adopted nebular parameters and errors, choices about which ion abundance to adopt were made when the values differed.

In order to derive overall elemental abundances, corrections must be made for the unobserved ion stages. The ionization correction factor (ICF) scheme we employed is taken from KB94, which in turn is based on detailed (unpublished) photoionization models for 10 PNe by Walton, Barlow, Monk, and Clegg. The abundances of neutral species were not derived; the fractions of neutral to ionized abundances are assumed to be the same as for hydrogen, in which case the final abundance ratios with respect to hydrogen are not affected.

Table 8 presents the adopted ion abundances, ICFs, and elemental abundances for each PN, along with the Webster (1988) excitation class and the KB94 PN Type classification. Uncertain results are indicated with quality codes. Following the ICF scheme of KB94, $A(S^{2+})$ values were estimated if the [S III] fluxes could not be measured. Listed separately in Table 8 are the abundances calculated for the low-ionization PNe, which are not included in further analysis. Low-ionization PNe are defined to be those with very low He Ifluxes and $A(O^+) > A(O^{2+})$; with much neutral material expected to be present, abundances for these nebulae cannot be calculated using our ICF scheme. The quality comment 'ul' indicates that the abundance should be considered an upper limit, as these are derived from very low S/N lines. From the simulations of Rola & Pelat (1994) the measured fluxes from low S/N lines are more likely to be overestimated than underestimated, by as much as 50 per cent at a S/N of 3. For any low S/N 4363 and 5755 Å lines, the derived T_e values could then be too high, hence the abundances too low. Any such uncertain T_e have been indicated in Table 6.

Some PNe were included in all three of our surveys. In Table 4 all sets of the measured fluxes are given, but in Table 8 results from only the adopted one are presented; usually one of the spectra was of better quality than the others. Taken from the FLAIR II survey are IC 4673, H 1–20, M 1–42, M 2–23, M 2–27, M 1–27, M 1–29, and M 2–29, and taken from the Middlemass spectra are M 2–20, H 1–54, M 2–30, H 1–63, and H 1–55. Excluding M 2–20 (with low s/n spectra) we find that the individual abundances usually agree within about ±0.2 dex, or ±0.01 by number for He/H, with only argon showing systematically higher values derived from the FLAIR II spectra. The argon abundances are uncertain anyway, as the ICFs assume a great importance.

3.3 Sources of uncertainty in the derived abundances

We consider two sorts of uncertainty; propagated flux measurement errors, and methodological errors. Later we discuss systematic biases and selection effects.

Table 9. Estimated ionic and elemental abundance errors. For helium these are given as percentages, for the others in dex.

He^+:	±5	S^{2+}:	$^{+0.20}_{-0.30}$	Ne/H:	$^{+0.20}_{-0.40}$
He^{2+}:	±5	Ar^{2+}:	$^{+0.08}_{-0.10}$	Ar/H:	$^{+0.44}_{-0.40}$
N^+:	$^{+0.18}_{-0.15}$	Ar^{3+}:	$^{+40}_{-25}$	S/H:	$^{+0.44}_{-0.30}$
O^+ 3727:	$^{+0.44}_{-0.30}$	Ar^{4+}:	$^{+0.10}_{-0.12}$	N/O:	$^{+0.23}_{-0.50}$
O^+ 7325:	±0.30	Ne^{2+}:	$^{+0.13}_{-0.22}$	Ne/O:	$^{+0.14}_{-0.22}$
O^+ both:	±0.30	He/H:	±7	Ar/O:	$^{+0.44}_{-0.40}$
O^{2+}:	$^{0.15}_{0.22}$	O/H:	$^{+0.15}_{-0.22}$	S/O:	$^{+0.20}_{-0.50}$
S^+:	$^{+0.23}_{-0.19}$	N/H:	$^{+0.20}_{-0.40}$		

3.3.1 Formal errors

Formal ionic abundance errors were calculated by propagating errors in the flux, T_e, and n_e for the range of temperature and density encountered. The errors do not behave exactly the same for the four combinations of T_e and n_e that were used in deriving abundances, but they are similar enough that a mean could be adopted.

For total elemental abundances, the errors depend on the particular ions included for each PN. We therefore calculated average elemental abundance errors, these are listed in Table 9. In accordance with the standard notation for abundances, helium is given in this paper in linear units and thus the errors in Table 9 as percentages, whereas the metals are quoted in log units and errors thus in dex. Note that when converted into log units, the errors will become smaller in the positive direction than the negative direction. Note also that we have different levels of positive and negative (linear) errors for most of the ions, because of way the flux measurement errors affect the T_e and n_e values.

The uncertainties for the sulphur, and argon abundances are quite high, because of the importance of the ICFs as usually only trace stages are observed and often the lines are quite faint. The sulphur and argon ICFs make use of the very temperature-sensitive N^+ and O^+ abundances, which is therefore a source of uncertainty. Additionally, usually $A(S^{2+}) > A(S^+)$ but the uncertainty for the faint, and extremely temperature-sensitive [S III] 6312 Å line is quite high, as it is for cases where the value is assumed (as part of the ICF scheme).

3.3.2 Methodological errors

The most obvious source of methodological error is that inherent to the ICF scheme. ICFs allow the determination of abundances from limited data, and therefore do not provide a complete solution. Alexander & Balick (1997) investigated the errors that can be incurred when using the KB94 ICF scheme. For a range of input central star T_{eff} and L_* values, they find the following: $\leqslant$10 per cent errors for helium and oxygen, ±25 per cent for nitrogen, sulphur, and neon, and a systematic overestimate of the true argon abundance by >25 per cent. These uncertainties have not been included in our error estimates.

We compared the ICFs for each PN with their derived abundances, T_e and n_e values and line fluxes, to search for unexpected correlations. For argon the ICFs for the bulge PNe are on average higher than those for the disc PNe. This is because the ICF adopted depends on the number of argon ions detected, for the KB94 disc PNe more argon ions were detected than for the bulge PNe.

The abundances of O, Ne, Ar and S are expected to be determined only by the abundances in the ISM from which the precursor stars formed, and thus their ratios relative to oxygen should show no correlation when plotted against each other. We find that in general they

Table 10. Mean abundances for our bulge PNe and KB94 disc PNe. He/H ratios are by number, the rest are log (X/H) + 12.0. 'Bulge' values are a straight mean of the FLAIR II, Middlemass AAT, and AAT 1978 samples, the individual means of which (latter two combined) are also given. ± values in most cases are standard deviations *not* errors, but see the text for additional comments for the '*' negative standard deviation entries.

	He/H	O/H	N/H	Ne/H	Ar/H	S/H
			Bulge			
Type I(7)	0.123±0.03	$8.63^{+0.16}_{-0.26}$	$8.75^{+0.12}_{-0.17}$	$8.05^{+0.15}_{-0.23}$	$6.65^{+0.14}_{-0.21}$	$7.19^{+0.22}_{-0.46}$
non-Type I(38)	0.109±0.02	$8.67^{+0.18}_{-0.31}$	$8.28^{+0.27}_{-0.87}$	$8.03^{+0.25}_{-0.69}$	$6.59^{+0.22}_{-0.48}$	$7.01^{+0.28}_{-0.92*}$
All(45)	0.111±0.02	$8.66^{+0.18}_{-0.30}$	$8.43^{+0.27}_{-0.81}$	$8.03^{+0.24}_{-0.56}$	$6.60^{+0.21}_{-0.41}$	$7.05^{+0.27}_{-0.83}$
			Disc			
Type I(11)	0.128±0.04	$8.65^{+0.12}_{-0.17}$	$8.74^{+0.16}_{-0.25}$	$8.09^{+0.13}_{-0.18}$	$6.42^{+0.15}_{-0.24}$	$6.98^{+0.16}_{-0.27}$
non-Type I(43)	0.112±0.02	$8.68^{+0.16}_{-0.27}$	$8.12^{+0.21}_{-0.43}$	$8.08^{+0.18}_{-0.32}$	$6.40^{+0.28}_{-0.43*}$	$6.91^{+0.19}_{-0.34}$
All(54)	0.116±0.02	$8.67^{+0.16}_{-0.26}$	$8.34^{+0.28}_{-0.78*}$	$8.08^{+0.18}_{-0.30}$	$6.42^{+0.26}_{-0.43*}$	$6.93^{+0.18}_{-0.31}$
FLAIR II(32)	0.108±0.03	$8.67^{+0.18}_{-0.32}$	$8.39^{+0.25}_{-0.68}$	$8.09^{+0.23}_{-0.54}$	$6.65^{+0.20}_{-0.38}$	$7.05^{+0.24}_{-0.58}$
Middlemass(13)	0.112±0.02	$8.63^{+0.16}_{-0.26}$	$8.51^{+0.28}_{-0.77*}$	$7.92^{+0.23}_{-0.52}$	$6.45^{+0.21}_{-0.40}$	$7.09^{+0.35}_{-0.58*}$
Solar[a]	0.098±0.008	8.69±0.05	7.92±0.06	8.08±0.06	6.60±0.06	7.33±0.11
H IIlocal[b]	0.10	8.70±0.04	7.57±0.04	7.9±0.1	6.42±0.04	7.06±0.06
H IIdisc[c]	0.10	$8.75^{+0.19}_{-0.35}$	$7.55^{+0.26}_{-0.42}$	$7.84^{+0.11}_{-0.19}$	$6.49^{+0.19}_{-0.32}$	$7.14^{+0.15}_{-0.24}$

a: Grevesse & Sauval (1998). O/H from Allende et al. (2001). ± are errors.
b: H ii regions, taken from Vílchez & Esteban (1996), for the solar neighbourhood. ± are errors
c: H ii regions, taken from Shaver et al. (1983) for the whole Galactic disc. ± are standard deviations.

do not. However, for the bulge PNe a positive correlation (correlation coefficient $r \sim 0.7$) between Ne/O and Ne/H is found, and for both sets of PNe positive correlations ($r = 0.7$–0.8) between S/O and S/H, and Ar/O and Ar/H, are found, with slopes of 0.5–0.8, although the scatter is high. We cannot identify the source of this, and so do not investigate these relationships any further.

4 ABUNDANCE DISTRIBUTIONS

Table 10 presents mean abundances by number for the bulge and KB94 disc PNe, by number relative to hydrogen on a logarithmic scale with H = 12.0, except for He/H. PNe considered to be incompletely ionized, judged as those having $O^+/H^+ > O^{2+}/H^+$ and low He/H ratios, have been excluded. For comparison, also given are solar abundances taken from Grevesse & Sauval (1998), and Allende Prieto, Lambert & Asplund (2001) and mean abundances for H II regions – a Galactic disc mean taken from Shaver et al. (1983) and a solar neighbourhood mean taken from Vílchez & Esteban (1996). Table 11 presents the N/O and Ne/O values for our two PN samples.

Table 11. Mean abundance ratios. Solar and H II region values are taken from the same references as for Table 10. He/H and N/O and Ne/O are given in linear units, while O/H is in log (H=12.0) units. The ± values are the standard deviations, except for the solar entries, which are the published uncertainties. For N/O, the positive and negative standard deviation values were calculated differently; see text.

	He/H	O/H	N/O	Ne/O
bulge TyI(7)	0.123	8.63	$1.1\pm0.25^{+}$	0.28±0.09
disc(11)	0.128	8.65	1.3±0.5	0.28±0.10
bulge non-TyI(38)	0.109	8.67	$0.35^{+0.22}_{-0.23}$	0.22±0.09
disc(43)	0.112	8.68	$0.29^{+0.17}_{-0.18}$	0.26±0.09
bulge All(45)	0.111	8.66	$0.68^{+0.77*}_{-0.56}$	0.23±0.09
disc(54)	0.115	8.67	$0.50^{+0.48}_{-0.39}$	0.26±0.09
Solar	0.098	8.69	0.17±0.02	0.25±0.02
disc H II	0.100	8.70	0.06±0.02	0.19±0.10

*see text, +calculated excluding Ae 1-1

Except for the solar and local H II region entries, also given in Tables 10 and 11 are the standard deviation values calculated for the whole bulge and disc sample. The usual formula for standard deviation, however, does not deal adequately with samples with significant skew in them, with the result that for some entries of Table 11, the standard deviations exceeded the actual value (and a negative abundance is of course, nonsense). To account for this for N/O we quote rather as the negative 'standard deviation', the difference between the mean value and the 5th smallest in the sample. For the PNe (but not for the H II regions) in Table 10, for some entries we quote this 'standard deviation' as well, if less than an unacceptably large original value; specifically for some of the N/H abundances, which Fig. 4 (later) shows not to have a Gaussian distribution, as well as Ar/H and S/H, which have some entries with very high standard deviations (adopting however the third smallest value in the small 'Middlemass only' sample). The distribution functions (see below) provide a better understanding of the width of the sample distribution, but we give here standard deviations as they are useful to compare to those quoted by other surveys and allow an easy comparison to the errors.

Fig. 3 presents several log–log plots showing the relationships between a number of abundance ratios. Fig. 4 presents plots of the abundance ratios in histogram form, as distribution functions (DFs).

In the following discussion the abundance distributions of the elements are compared for the bulge and disc samples, and the relationships between elements tested for correlations. To aid this, various statistical tests have been carried out on the data (excluding upper or lower limits). To test for correlations we used the value of the correlation coefficient, r, for which a value $\geqslant 0.6$ indicates a probable real correlation (most reliably for linear correlations). To test for the probability that the two samples of data are likely to be drawn from the same population we used the *Mann–Whitey U-test* (adapted from Press et al. 1992) and included also a test of the mean (*Student's t-test*) and dispersion (*f-test*). For the DFs, we also carried out a χ^2 test on the similarity of the two samples, as well as a *Kolmogorov–Smirnov* type test (one can consider this to test the similarity of cumulative DFs). This test in particular shows that the distributions of He/H, O/H, N/H, and S/H data are not statistically different between the bulge and disc samples.

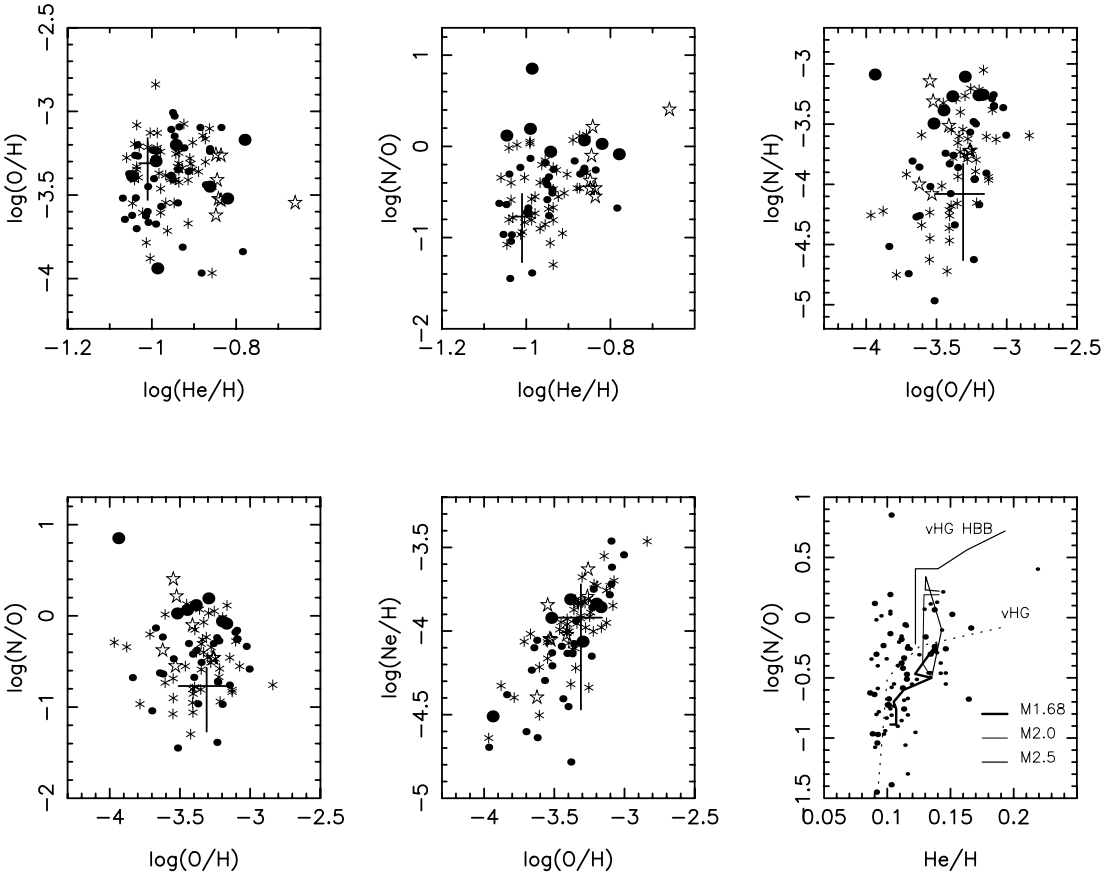

Figure 3. Plots of bulge PN (dots) and disc PN (asterisks) abundances. Type I PNe are identified as the larger symbols (big dots and stars), non-Type I as small symbols. The 1σ error bar (see Table 9) is shown at the solar value. The bottom right plot shows theoretical tracks taken from van den Hoek & Groenewegen (1997) (vHG) for their prescription, including a metallicity-dependent treatment of the AGB evolution and a Galactic disc chemical evolution model, both with (marked HBB) and without hot-bottom burning. The tracks marked 'M' are taken from Marigo (2001) for three values of the mixing-length parameter for solar metallicity progenitor stars. The direction of increasing He/H and N/O is more-or-less that of increasing precursor mass, ranging approximately from 1.3–5 $M_{\odot}$ for the thick line, and 3–5 $M_{\odot}$ for the other two lines (see Marigo 2001, for more details). He/H is plotted here in linear units. Large points are the bulge data. The tracks were measured by eye from the respective papers and have thus been smoothed.

Additional testing was carried out, including the lower limits in our data sets (increasing both sample sizes to about 70); this included the incompletely ionized PNe, those for which the ICF could not be calculated, and those in Table 7. The He, O, N, and N/O data were tested with the survival analysis method (Feigelson & Nelson 1985), using the package 'twosampt' in IRAF. Unless otherwise stated in the following, all statistical tests showed no significant sample differences or correlations.

4.1 Helium

The He/H mean and standard deviation[4] values for the 7 Type I bulge PNe, 0.123 ± 03, and for the 11 Type I disc PNe, 0.128 ± 04, are the same within the errors (see Table 9). For the 38 non-Type I bulge PNe, the mean He/H ($\langle$He/H$\rangle$) is 0.109 ± 0.02, and for the 43 disc PNe, 0.112 ± 0.02, again the same within the errors. The DFs for both samples peak at the low values and have a tail to higher values (Fig. 4), with the bulge sample peaking at slightly lower values than the disc sample. All calculated statistics support the view that the two samples are not distinguishable from each other.

[4] The values quoted with the mean values are, unless otherwise stated, the standard deviations. Note that this is of limited relevance for the Type I subsamples because of their small size.

4.2 Oxygen

The bulge and disc PN $\langle$O/H$\rangle$ values are respectively $(4.68 \pm 2.40) \times 10^{-4}$ and $(4.79 \pm 2.13) \times 10^{-4}$ by number for the non-Type I nebulae, and $(4.26 \pm 1.91) \times 10^{-4}$ and $(4.47 \pm 1.43) \times 10^{-4}$ for the Type I nebulae. Becker & Iben (1979) predict an oxygen depletion for solar metallicity stars of 10 per cent as a result of the ON cycle during the 2nd dredge-up phase, and van den Hoek & Groenewegen (1997) also predict negative oxygen yield for higher mass post-AGB stars. Formally our values support this view, although within the errors the values are the same, and the small size of the Type I sample, and the large dispersion, should be taken into consideration. In addition, our plots of O/H versus He/H and N/O versus O/H show no negative correlations, as would be expected if the predicted oxygen depletion was present.

For the relationship of O/H with He/H, the population of the high He/H–low O/H end of the distribution is sparser than elsewhere, but not enough to lead to a correlation (compare the plot with that of N/O versus He/H, where a relationship is more obvious). In a

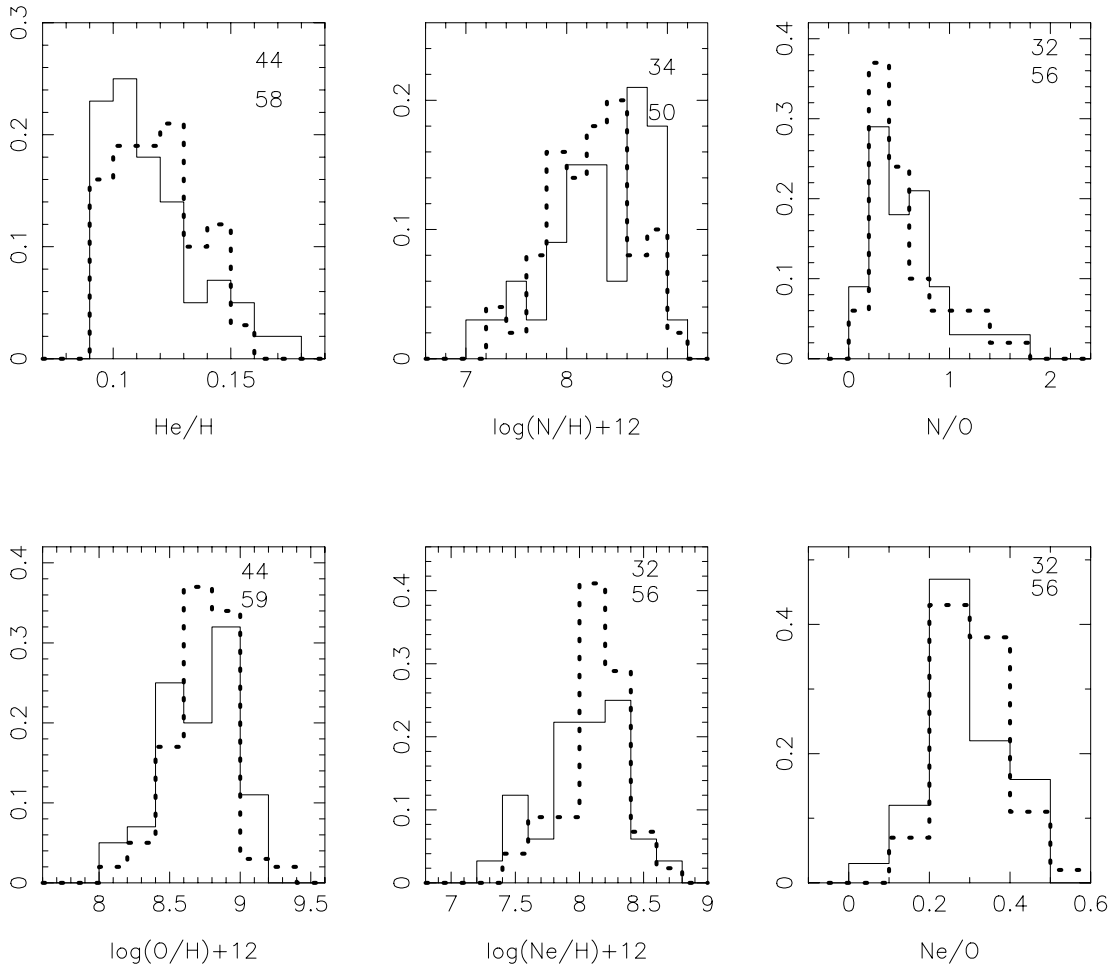

Figure 4. Bulge PN (solid line) and disc PN (broken line) abundance distributions. The histograms have been normalized to an area of 1 to aid comparison, the vertical axis scale is the fraction of nebulae in each bin. The number in each group is given on the plots, with the bulge given as the upper value. The N/O distribution has an unplotted bulge point at 7.4 and disc distribution a point at 2.8. All nebular types are included.

similar vein, the relationship between N/H and O/H does not show a correlation, as although formally a steep slope (about −2.6) can be measured, this does not really pass the thumb test (cover a small percentage of points with the thumb; if a trend disappears it was probably not real).

The disc O/H DF is narrower than that of the bulge. A Gaussian fit results in a full-width at half-maximum (FWHM) of 0.64 dex and 0.44 dex for the bulge and disc samples respectively. The standard deviations similarly differ (see Table 10), at 51 and 44 per cent respectively. The data plotted in a cumulative DF also support the view, nicely, that the mean values of the bulge and disc O/H data are the same, but they differ slightly in dispersion. While it is true that the errors for the disc PNe are generally lower than for the bulge PNe – KB94's greater wavelength range resulting in more ions being observed – for oxygen this difference is expected to be slight (the bright [O III] lines and the ICF-important He lines are well observed).

If there were only one true value of the oxygen abundance for all PNe, and the scatter in our data resulting from a Gaussian distribution of errors, we should find a FWHM of about 0.44 dex[5] and that 50 per cent of the abundances lie within the probable error:[6] this is true for the disc PNe, but not for the bulge PNe where only 38 per cent do. Thus, there is a slight indication that the bulge O distribution width exceeds that resulting from errors, or that the errors are underestimated. There are also additional factors that can broaden the oxygen distribution, considered below, and which require detailed modelling if they are to be taken into account. The difference in the disc and bulge oxygen dispersions is small and our statistical tests show no significant difference in the two samples. Conservatively, we therefore will assume that the widths of both oxygen distributions are caused by errors and are the same. The same level of scatter is expected also for neon and nitrogen, elements for which the ICF errors are assumed to follow those of oxygen (although the formal errors for individual PN in Table 9 are higher), and thus the scatter in the oxygen data can determine the errors expected for these also.

Various factors influence the widths of the oxygen DFs. For the disc PNe, a Galactic radius increment of 4 kpc (taking the distances for the subsample of PNe in Kingsburgh & English 1992) would give a contribution to the total scatter in the mean O/H of about 0.28 dex

[5] Determined adopting a 40 per cent error (σ) and a Gaussian FWHM of 2.35σ.

[6] If the distribution about a mean value is Gaussian, then 50 per cent of the abundances should lie between the mean and $\pm 0.6745 \times \sigma$, where σ is the abundance error.

for the Galactic O/H radial gradient of Rolleston et al. (2000), less than the contribution from the errors. It is uncertain if there is an abundance gradient in the bulge (Feltzing & Gilmore 2000; Wyse 1999; Minniti et al. 1995), evidence therefore seems to be based on comparisons between several Schmidt fields on Baade's Window with other directions; our bulge data are from only two fields in Baade's Window.

In addition, one should consider any evolution of the oxygen abundance with time. The highest progenitor mass PN would have abundances exceeding those of the Sun, in the presence of an age–metallicity relation. In the disc, star formation is an ongoing process, but the age–metallicity relation is observed to have a considerable scatter, being a few tenths of a dex at any age (Edvardsson et al. 1993). Intermediate-age stars have the entire range of Fe/H abundances, a decreasing age with increasing Fe/H being found for the oldest and youngest stars only (Wyse 1999). Chemical enrichment of the galaxy is obviously an inhomogeneous process. The scatter in H II region abundances at any particular galactocentric radius is, according to Shaver et al. (1983), less than 20 per cent rms. In summary, the scatter in our oxygen distributions will be affected by Galactic evolution, but at a level that probably does not exceed our errors. According to Matteucci & Romano (1999), star formation is believed to have ceased in the bulge, with none occurring in the last 5 Gyr, and with most stars being older than 10 Gyr. If this was true, there should be less scatter in the bulge DFs from evolution of the oxygen abundance than for the disc DFs. We find no difference between the oxygen abundances of the Type I and other PNe in either the disc or bulge PN samples, so unless the Type I classification fails to pick out the higher mass precursor stars, this would argue against any noticeable evolution in the oxygen abundance with time for either the disc or bulge PN progenitors (although at the same time, the presence of Type I PNe indicates relatively recent star formation).

The mean O/H for both the bulge and disc PNe shows excellent agreement with the solar value of $\log(\mathrm{O/H})+12 = 8.69$ recently determined by Allende et al. (2001). With respect to disc H II regions, the PNe are only slightly less abundant in oxygen, by 0.03–0.04 dex. Henry (1998) plotted O/H versus galactocentric distance for PNe, H II regions, and B stars, finding that the PNe in his sample had systematically lower abundances than the H II regions at corresponding radii, by about 0.14 dex, which he interpreted as arising from the PNe being older and less metal-rich.

4.3 Nitrogen

The $\langle \mathrm{N/H} \rangle$ values for the Type I bulge and disc PNe, $(5.62 \pm 1.79) \times 10^{-4}$ and $(5.50 \pm 2.45) \times 10^{-4}$ respectively, are similar and they are naturally significantly enriched compared with the non-Type I PNe, the values of which are respectively $(1.91 \pm 1.64) \times 10^{-4}$ and $(1.32 \pm 0.82) \times 10^{-4}$. The mean N/H for all bulge PNe is ∼20 per cent larger compared with the disc PNe, and the DFs show that the bulge PN distribution does peak at higher values (log values 8.6–9.0) than the disc PN distribution (8.2–8.6). The difference however is just outside the 1σ bin error (about 30 per cent at 8.7 dex). Our statistical tests do not allow us to conclude that there is a difference between the bulge and disc PN nitrogen distributions.

The dispersion in N/H for both samples is larger than the errors, being 81 per cent in the bulge sample (excluding Ae 1-1, which has a very high N/O ratio of 7.1 – an object worthy of closer study), or 90 per cent for a subsample of best-quality spectra, and 90 per cent for the disc sample. Both nitrogen DFs have a tail to low values, neither therefore being of Gaussian form. However, we can estimate the broadening of the nitrogen DFs by fitting Gaussian profiles to the main peaks. If we assume the only contributions are the intrinsic broadening and the contribution arising from errors, we can estimate the former. Fitting Gaussian profiles to the (log) nitrogen DFs, we obtain peak and FWHM values of 8.5(1.2) and 8.3(1.1) for the bulge and disc PNe respectively. Comparing our results with the oxygen DFs (previous section), which measure the broadening owing to errors, this leads to an intrinsic FWHM of about 1 dex for both samples. This is most likely the contribution from the mass range of progenitor stars (and consequent differences in the nitrogen enrichment), and from any evolution in the nitrogen abundance over time. Note that the nitrogen abundance gradient for the disc is slightly steeper than that measured for oxygen, -0.09 ± 0.01 dex kpc^{-1} according to Rolleston et al. (2000).

Previously we discussed the lack of evidence for significant O-enrichment via O→N cycling in our sample of PNe, such as could occur as a consequence of the second dredge-up. Enhancement of nitrogen occurs because of CN cycle products brought to the surface by the 1st dredge-up, predicted to occur for all LIM stars. Additional nitrogen can be produced via hot-bottom burning (HBB) of dredged-up carbon, which occurs for sufficiently massive stars following the third dredge-up (about >3.5 $\mathrm{M}_{\odot}$ according to van den Hoek & Groenewegen (1997), leading to higher nitrogen abundances in the Type I PNe. During CNO cycling the total number of CNO nuclei is conserved: if the oxygen abundance is not changed then one C atom becomes one N atom. KB94 compared their disc PN nitrogen abundances with the C+N abundances of Galactic H II regions (adopting the solar neighbourhood value, see Table 4), on the basis that these represent the initial C+N values for the PN progenitors, and compared their results with the predictions of Becker & Iben (1980). We can repeat this test for our bulge PNe, adopting the same initial C and N values as did KB94, as separate values are not known for the bulge, using the more recent predictions of van den Hoek & Groenewegen (1997).

In order to obtain the observed mean N/H values of 1.61×10^{-4} and 5.56×10^{-4} for the non-Type I and the Type I PNe, respectively (bulge and disc values averaged), about 40 per cent and 170 per cent of the original carbon would have had to have been converted into nitrogen. Following the first dredge-up, van den Hoek & Groenewegen predict an increase in the nitrogen abundance by 28 per cent for a 1 $\mathrm{M}_{\odot}$ star, and 37 per cent for a $\geqslant 3$ $\mathrm{M}_{\odot}$ star, from CN-cycle conversion of part of the original carbon abundance. Obviously, for the Type I PNe more carbon conversion is required; again we infer that this 'extra' carbon comes from the third dredge-up and is then converted to nitrogen by hot-bottom burning.

4.3.1 The N/O ratio

The mean and standard deviation of the N/O ratios for the Type I disc and bulge PNe are very similar to each other if Ae 1-1 (which has a very high value) is excluded from the bulge sample; by number $\langle \mathrm{N/O} \rangle = 1.13 \pm 0.28$ for the bulge Type I PNe compared with 1.26 ± 0.49 for the disc Type I PNe. For the whole bulge sample excluding Ae 1-1 (hence the difference with the value in Table 11), $\langle \mathrm{N/O} \rangle$ is 0.49 ± 0.38; the same as the disc value, $0.50^{+0.48}_{-0.39}$.

For the bulge sample (excluding Ae 1-1), the dispersion about the mean for all PNe (and for the subsample of those with the highest quality spectra) is 77 per cent, while we find 94 per cent for the disc sample. The latter is larger than the 70 per cent formal error; as with the N/H ratio, this could be a consequence of the mass range of the progenitor stars. We note that the N/O ratio, which is sensitive to the mass of the precursor star, has a very similar

distribution in the bulge and disc PN samples (Fig. 4). The statistical tests show that the N/O DFs for the bulge and disc PNe are not significantly different (however, see the later discussion on selection effects).

Becker & Iben (1980) pointed out that primordial variations of a factor of 2 in C/O and N/O will introduce a factor of 2 to 4 variation in the N/O ratio found in nebulae from low-mass stars ($<2.25\,M_{\odot}$), and that therefore a spread in N/O of the order of 0.6 dex (a very large dispersion and comparable to the scatter in our values: Fig. 3) is expected anyway in nebulae showing only modest enhancements of helium ($\sim$0.01).

4.3.2 N/O versus He/H

Since the N/O ratios and He/H abundances are affected by nucleosynthesis and dredge-up in the progenitor star, it is useful to compare the observed relationship between these parameters with the predictions. Our distributions of N/O versus He/H for the bulge and disc PNe are not statistically different to each other, as there are also no significant correlations between the two parameters ($r\sim$0.4). However there is a shape to the relationship, as can be seen on Fig. 3. The N/O versus He/H plane can be divided into three sections. At low N/O there are only PNe with low He/H values. At high He/H there are no low N/O values. At high N/O values the complete range in He/H is sampled (or at low He/H values the full range in N/O is covered). The split in N/O occurs at $\sim$0.25 and in He/H at $\sim$0.125. There is no difference in the distribution of He/H values between the Type I PNe and the non-Type I PNe located above N/O $\sim$ 0.25. This could suggest that the second dredge-up, which operates in the higher mass stars, does not have an important effect on the helium abundance.

Following from this, we then compared the other mean abundances and their relationships for a subsample of objects with very high helium abundance, He/H $>$ 0.14, to those with lower He/H values. For the bulge PNe no significant differences are found in the mean abundances – the four such objects have a higher mean N/H (0.12 dex) and S/H (0.32 dex), but in light of the small number of these objects and the abundance errors, this is not significant. For the disc sample, however, we do find some striking differences. The seven such PNe have a mean N/H that is 0.5 dex higher and a mean (linear) N/O that is 128 per cent higher (and a mean C/H 0.33 dex lower) than the subsample with lower He/H abundances. This mimics the relationship already discussed, where at high He/H values only high N/O values are found.

For the other elements, the similar abundances found for the low and high helium abundance disc PNe suggests the same initial metallicity for these PNe, although stellar and Galactic evolution models would be required to check that these two conditions must always follow each other. Although there is a lack of marked distinction in the He/H abundances for Type I PNe compared with the rest, and the bulge and disc samples have the same distributions as each other, it is possible that the highest He/H and N/O disc PNe (see above), which may come from the highest mass precursor stars, find no counterpart in the bulge population. We stress, however, that this suggestion is based on a very small subsample of high helium abundance PN.

At the bottom right of Fig. 3 we repeat the N/O versus He/H plot and include theoretical tracks taken from Marigo (2001) and van den Hoek & Groenewegen (1997); the latter's tracks incorporate a model of the chemical evolution of the Galactic disc and various improvements on preceding models for the 2nd dredge-up and for the HBB phase (their Section 3). Their track including HBB far exceeds the range of our data, although it does explain the high N/O objects well (but not those also with low He/H values). Their track without HBB follows the trend of most of the rest of our data well, up to the point where the HBB and no-HBB tracks meet. Similarly, the tracks of Marigo (2001) define the lower-right envelope of our data and the extension to high He/H and N/O, but do not predict objects with low He/H and high N/O.

4.4 Neon, argon and sulphur

Argon and sulphur abundances are subject to greater uncertainty than those for the other elements, mainly because of their large ICFs. Neon is uncertain because [Ne III] 3868, 3967 Å fall on a less well calibrated region of the spectrum and the latter is sometimes blended with neighbouring lines, although Ne^{2+} is usually a dominant ion, and thus representative of most of the neon abundance. All three elements show unexpected correlations, discussed in Section 3.3.2. Hence, our results for these elements will not be discussed in as much detail as for the previously discussed elements, and only plots of the neon abundances are provided in Figs 3 and 4.

The bulge and disc Type I and non-Type I PN samples all have the same mean S/H, Ne/O and S/O ratios as each other, within the errors. For Ne/H and S/H the standard deviation of the bulge sample is wider than that of the disc sample (70 per cent compared with 50 per cent, and the bulge has more PNe at low values) and just larger than the error (60 per cent), although most statistical tests on the distributions do not support their being significantly different. The *Kolmogorov–Smirnov* statistic, however, suggests that the bulge and disc neon abundance distributions do differ. Looking at the DF of Fig. 4 suggests that the wider DF for the bulge data, and the relatively higher number of low Ne/H PNe therein, is the cause of this. Unfortunately, higher errors could account for this; the KB94 PN have lines of Ne^{3+} and Ne^{4+} in their abundance calculations that we do not.

Following Henry (1989) we looked at the relationship between Ne/H and O/H. Henry found a lockstep relation (slope unity when plotted in log-log format) between the two for PNe and H II regions in a number of galaxies. This suggests that neither element has been affected by the nucleosynthesis in the precursor stars. We also find such a relation (Fig. 3), however, unlike Henry's case, our bulge PNe show an unexpected positive correlation between Ne/O and O/H. These two elements are related by their ICF, and this correlation suggests a spurious relationship between the two elements dictated by the ICFs, although only a few of the bulge PNe have both high ICF(Ne) and high Ne/H abundance. The disc PNe show no such correlation, and hence we do not place much weight on our lockstep relation.

4.5 Summary

We find the following.

(i) Little significant difference in either the mean abundances, their dispersion, or their relationships for the bulge and disc PN samples. Small differences will be masked by the errors and especially by the various uncertainties that exist for PN abundances derived from CELs (see below). However, the same analysis methods used for the bulge and disc PNe should rule out most systematic biases being important.

(ii) The width of the nitrogen distribution, of all elements, most likely exceeds that arising from errors.

(iii) We find that at high He/H values there are relatively fewer low O/H, N/H and Ne/H abundance PN than high abundance PN. For O and Ne, the trend is not significant enough to define a true correlation.

(iv) On the N/O versus He/H plane, however, the trend *is* significant enough to define a true correlation.

(v) There is no evidence for oxygen depletion for the Type I PNe compared with the rest, although a small (10 per cent) difference is not excluded.

(vi) It is possible that the dispersion in the disc PN oxygen and neon abundances is less than that of the bulge. However, other factors of importance in the dispersion – the galactic abundance gradient, any age–metallicity relation – should be considered. Given the many factors of importance, to use similar data to ours to study them much larger samples (to allow for lower statistical errors) are recommended.

(vii) The theoretical tracks overplotted with our data on the N/O to He/H plane do not explain the PN with high N/O ratio and low He/H abundance.

(viii) The disc PN with He/H > 0.14 have significantly higher N/H and lower C/H than the rest, which is not found for the bulge PN. This is, we note, based on only a handful of objects.

5 UNCERTAINTIES

Due consideration of the selection effects and systematic errors is important; we need to know if there are any types of PN and abundance ranges that are selected against. In this section we briefly discuss some of the selection effects that could affect our conclusions, and in the Appendices discuss searches for more specific biases within our data sets.

5.1 General

For the purpose of our *comparative* study, it is enough if systematic errors do not distinguish systematically between the bulge and disc samples, since the same methods were used to derive both sets of abundances. The Middlemass PNe were selected to be of low excitation, and therefore have a bias; this can be noticed in the trend for the bulge PN sample to extend to higher T_e and lower n_e values than do the Middlemass sample of PNe. We do not find this to affect the distribution of the abundances or the relationships of Figs 3 and 4, outwith of the errors.

For the FLAIR II sample no selection criteria were used other than to observe as many PNe as possible during the observing run. There were likewise no selection criteria for the KB94 disc PNe. Other selection effects operate over which we have no control. We have already pointed out that the larger and fainter objects will be selected against in the bulge. Another consideration is the expectation that the brightest PN come from a slightly metal-poor population (Ciardullo & Jacoby 1992). Also, low-mass central stars that do not get hot enough to ionize the nebula will become 'invisible' PNe, leading to a selection against the oldest objects, and indeed a study of the selection biases for GBPNe by Stasińska & Tylenda (1994) finds that the observed central star mass distribution is biased slightly upwards of the intrinsic one. Another possible bias could be against the very high-metallicity objects; and given the different star formation histories of the bulge and disc, this may affect our two samples differently. In studies of stellar evolution at high metallicity (e.g. $Z = 0.1$) it is found that the mass loss rate (at all stages) is increased, and luminosity, $T_{\rm eff}$, and lifetimes changed. In some cases, it is possible for an object that is a PN precursor at low metallicity, to, at high metallicity, avoid the AGB or later AGB stages altogether, and thus, if it produces a PN, produce a PN of different heavy-element abundances (Mowlavi et al. 1998; Greggio & Renzini 1990; Fagotto et al. 1994). This could result in a bias against the highest metallicity objects in our survey and be a source of confusion on Figs 3 and 4. Therefore, when comparing results such as ours with models of the chemical evolution of different parts of the Galaxy, these selection biases must be taken into account.

Table 12. A comparison of mean abundances from this paper with those from a variety of published works, for Galactic bulge and disc PNe. TPP77 is Torres-Peimbert & Peimbert (1977), W88 is Webster (1988), RPDM97 is Ratag et al. (1997), SRM98 is Stasińska et al. (1998), KB94 is Kingsburgh & Barlow (1994), SKAS92 is Samland et al. (1992), CMKAS00 is Cuisinier et al. (2000), EC91 is Escudero & Costa (2001), and AK87 is Aller & Keyes (1987). Apart from He/H, the abundances are in units of log X/H+12.0.

	He/H	O/H	N/H	Ne/H	Ar/H	S/H
bulge						
This paper (44)	0.111	8.66	8.43	8.03	6.60	7.05
SRM98 (80)	0.103	8.71	8.36	8.09		
RPDM97 (92)	0.120	8.79	8.52	8.16	6.62	7.00
W88 (54)	0.113	8.73	8.90			
CMKAS00 (30)	0.104	8.75	8.30		6.47	6.94
EC01 (45)	0.126	8.22	7.64		5.95	6.48
disc						
TPP77 (28)	0.112	8.87	8.33	8.28		
SKAS92 (57)	0.112	8.78	8.40		6.57	7.31
KB94 (51)	0.116	8.67	8.34	8.08	6.42	6.93
AK87 (43)	0.117	8.63	8.46	7.95	6.48	7.11
Comparison for PNe in common with this paper						
SRM98 (21)	0.115	8.65	8.41	8.14		
This paper (21)	0.111	8.70	8.26	8.05		
RPDM97 (21)	0.121	8.78	8.53	8.16	6.64	7.00
This paper (21)	0.112	8.66	8.32	8.03	6.61	7.01

5.2 T_e and n_e fluctuations

Many studies have looked at the effect on derived abundances of using values of T_e and n_e obtained from CEL ratios. It is now understood that there is a problem with the way most abundance derivations are made; nebulae are not homogeneous, and assuming they are can result in incorrect derived abundances (see Liu et al. 2000 for an analysis of this for NGC 6153). Temperature and density variations have been proposed as the cause of the difference (an underestimation) between CEL abundances and those derived from optical recombination lines. A good overview of this is provided in Rubin et al (2003) and it would be redundant to repeat it here. Unfortunately, consensus on the affect on the derived abundances has not yet been reached, and a standard set of corrections (particularly for unresolved PNe) is not available.

6 COMPARISON WITH OTHER PN ABUNDANCE SURVEYS

In Table 12 we compare mean abundances from previously published PN surveys (both bulge and disc) with our own.

(1) *Webster (1988)* derived empirical abundances for 54 bulge PNe, using the CEL ratios for the T_e and n_e calculations. Her oxygen ICF(O) was adopted to be the straight ratio of He/He^+, rather than the power of 2/3 as for our KB94 ICF scheme. Her helium

abundance calculation did not account for the collisional excitation of He I lines, allowance for which would have reduced her derived He/H values by about 9 per cent (bringing them into agreement with our own).

(2) *Samland et al. (1992)* derived abundances using a grid of photoionization models for a sample of 57 high-excitation galactic disc PNe.

(3) *Ratag et al. (1997)* analysed their own observations of 45 bulge PNe, and re-analysed published data on about 50 other bulge PNe. They adopted the same set of diagnostic line ratios as here with some additional ones for the electron density, but with slightly different selection criteria. Abundances were derived using a grid of photoionization models to predict the ICFs required for each PN. They did not publish their ICFs.

(4) *Stasińska et al. (1998)* adopted fluxes for 80 bulge PNe from a variety of sources, and followed a similar empirical abundance derivation scheme to our own – using the KB94 ICFs – however they favoured T_e(O III) unless only T_e(N II) was available, and rejected the 7325 Å determined values of A(O^+) in favour of those from the 3727-Å line, when possible.

(5) *Cuisinier et al. (2000)* derived abundances for about 30 bulge PNe from spectrophotometric data, using the same empirical methods as us and deriving abundances with their own ICF scheme, which for N, Ne and He are the same as ours. We have used only their abundances without the ':' quality code.

(6) *Escudero & Costa (2001)* reported on an abundance survey of 45 bulge PNe selected from recently discovered objects (not overlapping previous surveys, including our own). They used an ICF scheme to derive abundances from their optical spectra, using the red [O II] lines in preference to the blue ones for the O^+ abundance.

Mean abundances from the surveys compared here are given in Table 12. The numbers in brackets indicate the total sample sizes, though for some elements the number of nebulae involved is smaller than the overall sample size. In this table we do not quote the standard deviation values. This is because of the different sample sizes (particularly for elements other than He, O, and N) and the fact that several of the standard deviation values calculated for the entries of Table 12 were very large (exceeding 100 per cent). The range of standard deviation values – calculated using all the entries in the respective papers – is wide for all elements, being 17–43 per cent for He/H, and from about 50 per cent to over 100 per cent for all other elements. Therefore, to make a detailed comparison for data from different publications, figures such as Figs 3 and 4, possibly weeding out some entries (e.g. the incomplete ionized nebulae) are strongly recommended.

6.1 Comparison of mean abundances

There are a number of individual values that stand out in Table 12. The mean He/H for the Ratag et al. (1997) sample is higher than the others. Excluding this outlier, the range of values covered by all samples for He/H by number is 0.01 and $\leqslant$0.2 dex for the other elements, for both the bulge and disc samples.

The He/H ratios of the bulge PNe tend to be slightly lower than those of the disc PNe, while their O/H values tend to be slightly larger than those found for the disc PN samples. However, the mean O/H values found for our own bulge PN sample and the disc PN sample of KB94 agree to within 0.01 dex – these two samples were analysed using identical ICF procedures.

One survey that does stand out as having different results from the others is that of Escudero & Costa (2001). Compared with our results, their mean abundances are all lower by $\sim$0.5 dex (or 0.8 dex for N/H), except for He/H, which is higher (0.125). They noted that their O/H distribution is biased to lower values compared with those in the literature, similarly but less so for N/O. They suggested that was due to the different sky coverage, theirs spanning a greater range. Their PNe, located in a bulge region not studied before, are either thick disc objects or true bulge objects. They suggest that their lower mean abundances indicate a vertical abundance gradient within the bulge. We note that the dereddened Hγ fluxes of Escudero & Costa (2001) show an extremely large scatter about the mean value of 47 (on a scale where H$\beta = 100$) that is expected for Case B recombination. Since the key [O III] 4363 Å T_e diagnostic is adjacent in wavelength to Hγ, this suggests that the observational errors may be particularly large for the derived [O III] electron temperatures and the resulting oxygen abundances. Re-observation at higher S/N of the PNe for which they obtained their intriguing results would therefore seem desirable.

6.2 Differences for individual PNe

13 PNe were chosen at random to compare the abundances derived from our FLAIR II, Middlemass 1990 or AAT 1978 spectra with those derived by Stasińska et al. (1998), Ratag et al. (1997), or KB94 (these averages are not included in Table 12).

For each element relative to hydrogen, the variation about the mean, and its standard deviation, over this group of PNe was found to be about 30 $\pm$ 20 per cent for all elements except helium, for which it was 7 $\pm$ 6 per cent. For the Ne/O, Ar/O and S/O ratios, the scatter was 30 $\pm$ 30 per cent, and for N/O it was 50 $\pm$ 35 per cent. There are no systematic differences for any particular PN (over the individual elements) or for any particular element (over the individual PNe), except for helium which is always higher in the Ratag et al. data set. In most cases, the scatter is due to differences in the ICFs, especially for the N/O ratio; the ICF for nitrogen is based on the ratio A(O)/A(O^+), which can vary quite significantly, depending on whether A(O^+) was selected to be from the 3727 Å or 7325 Å lines of [O II].

7 DISCUSSION

7.1 The N/O ratio

Several published studies have compared the elemental abundance distributions of disc and bulge PNe, looking for differences between these two regions of the Galaxy. A major work was by Ratag et al. (1992), who compiled an inhomogeneous data base of 92 PN abundances. They found that the bulge PN abundances were considerably higher than predicted by the extrapolation of the disc abundance gradient. Their bulge and disc abundances showed similar distributions, except for helium and nitrogen which were both higher in the bulge. They suggested that the $\sim$40 per cent higher mean N/O in the bulge (due largely to a relatively longer tail to high N/O values) was due to the presence of more low-abundance PNe with high N/O values, rather than a higher average N/O ratio (which normally suggests higher mass, younger objects) and proposed an evolutionary scenario for the bulge in which there was more efficient star formation and a much shorter time-scale to collapse, with an initial mass function biased to less massive stars than in the solar neighbourhood.

Cuisinier et al. (2000) found a different bulge nitrogen distribution. They compared the N/O distribution function for their sample of 30 bulge PNe with that for 198 nebulae in the disc PN sample of Maciel & Köppen (1994), who had used the same ICF prescription.

They found that there were fewer bulge PNe than disc PNe with high N/O ratios – the former extending to a (linear) value ∼0, the latter to ∼0.5 – and interpreted this as being due to a deficit of higher mass progenitor stars in the bulge compared with the disc.

However, as discussed in Section 4.3.1, our own comparison between the N/O number distribution functions for 32 bulge PNe and 56 disc PNe that utilized the same ICF prescriptions (Fig. 4) shows the two samples to have the same distribution functions within the uncertainties – with the formal difference in mean values being small – i.e. no deficit or excess high N/O nebulae in the bulge sample compared with the disc sample. We see no strong evidence that He/H increases with N/O; rather Fig. 3 shows that at low N/O values (<0.25) only the lower He/H values (<0.125) are populated, but at high N/O values the whole He/H range is covered. The 12 bulge PNe and 19 disc PNe with N/O < 0.25 and He/H < 0.125 have essentially the same mean O/H ratio, 4.94×10^{-4} and 4.99×10^{-4} respectively, as the whole sample. Our high N/O ratios for the Type I PNe are due to high N/H values, rather than low O/H values.

For the Stasińska et al. (1998) and Ratag et al. (1997) samples in Table 12, we have been able to compare their abundances in some detail with our own for the same PNe. We reclassified theirs according to the KB94 Type I criterion and incompletely ionized objects were removed from the Stasińska et al. (1998) sample.

Considering the 21 PNe in common between our own survey and that of Stasińska et al. (1998), different proportions are classified as Type I PNe. We assign Type I status to two PNe, whereas six PNe in the Stasińska et al. (1998) subsample would qualify for Type I status, with only M 1–42 in common. Our N/O ratios are generally lower because of lower ICFs for N.

There are also 21 PNe in common between our survey and that of Ratag et al. (1997), and in both 14 per cent are classified as Type I PNe, although again only M 1–42 is in common. It is again the nitrogen abundances that vary the most between the two sets of data, although in this case we cannot compare the ICFs because Ratag et al. (1997) did not present their adopted values.

For these comparisons, we have calculated the standard deviation values. Although, as discussed previously, the standard deviation may not always provide a meaningful statistic on skewed samples, in this case it does as we are comparing abundances derived for exactly the same PNe. In this case, we find that comparing our two samples with the other samples, the standard deviations are quite similar for each element for He/H (25 per cent), O/H (58 per cent) and N/H (88 per cent: although a lower scatter as well as lower average value is found for the KB94 PNe that the RPDM97 sample). The high scatter in the N/H values compared with the other elements is therefore repeated in these subsamples.

We conclude that the different findings of Ratag et al. (1992), Cuisinier et al. (2000) and ourselves (or indeed, any other particular combination of authors), especially for the N/O ratio, could be due to an additive effect of different ICF schemes, different criteria for selecting the line ratios for T_e and n_e determinations, and probably quite importantly, small number statistics. Our study shows that any differences between the bulge and disc PNe is small, and thus very large studies would be needed to be sure of the correct interpretation of the data. This is especially so for the N/O ratio.

7.2 The proportion of Type I PNe

As as well as having similar N/O distributions, the proportion of Type I to non-Type I PNe in the KB94 disc sample and our bulge sample is similar: 18 and 25 per cent. This could indicate fairly recent star formation in the bulge, <1 Gyr ago. This presumes the same criterion for Type I PN status, N/O > 0.8, applies to the bulge as KB94 determined for the disc. Linking a high N/O ratio to a higher initial mass and therefore lower age seems to be countered by evidence for the majority of the stars in the bulge being old (see discussion below). Reliable initial (C+N)/O ratios for the bulge PN population are required, but the only observational values that we could find are from H II region studies. Afflerbach, Churchwell & Werner (1997) (see also Simpson et al. 1995), carried out an infrared fine-structure line study of three H II regions located at R_G = 0–0.2 kpc (i.e. in the Galactic Centre region, rather than in the bulge proper). These were found to have an average N/H ratio of 2.6×10^{-4}, an O/H ratio of 15.5×10^{-4}, and N/O ratio of 0.26 (the average ratio is not equal to the ratio of the averages); in all cases consistent with a extension of the disc gradient. No suitable value for the initial C/H abundance of bulge PN precursors could be found. Casassus et al. (2000, not published) suggested it to be low, based on a study classifying the mid-infrared dust emission features of bulge and disc PNe. They found that <30 per cent of bulge PNe were C-rich, compared with ∼80 per cent in the disc, consistent with the well-known trend for a decreasing frequency of carbon stars with decreasing galactocentric radius. More data would be needed on the initial abundances appropriate for the progenitors of our PN sample for us to be able to set a reliable value for the initial (C+N)/O ratio for bulge PNe, but all of our data show the bulge and the disc PN samples to be very similar in the abundances of those elements that are believed to reflect their initial metallicities.

7.3 The age and metallicity of the bulge

The bulge has a distinct stellar population, including both RR Lyr stars and late M giants and OH/IR stars: that these classes of stars reside in the same volume is clear evidence for a wide range of metal abundances (McWilliam & Rich 1994). McWilliam & Rich find very similar [Fe/H] distributions (Fe/H with respect to solar) for bulge and solar neighbourhood K giants, although the bulge distribution is somewhat broader, containing more low-abundance objects than the disc sample. This result is consistent with our finding very similar abundance distributions for the bulge and disc PNe, especially for O/H. According to Minniti et al. (1995), the comparison between bulge and disc abundances for different (heavy) elements shows some to be enhanced, some not; the conclusion is that the chemical evolution in the two regions must have been different.

The mean age and its distribution for bulge stars are still uncertain. *HST* data on unevolved stars in Baade's window (Wyse 1999) indicate an age of only 5–10 Gyr for a mean metallicity of about 0.5 solar, and colour–magnitude diagrams of evolved stars show a large intermediate-age population younger than 10 Gyr. However, Feltzing & Gilmore (2000) found that the bulk of the bulge field stars are in fact old, comparable to the halo, with no significant young or intermediate-age stellar population, arguing that careful analysis of their *HST* colour–magnitude diagrams shows that contamination by foreground disc stars could account for any detected younger objects. Compared with the disc, the bulge is thought to have formed earlier and much more rapidly. A faster evolution (more efficient star formation) in the bulge would account for the lack of young stars and for the older ones having high metallicities (Matteucci & Brocato 1990). If this were to lead to differences in the elemental abundances and ratios for our bulge and disc samples, the differences would have to be quite small: the abundances of O, Ar, Ne and S are not (or at most, little) changed by nucleosynthesis in the precursor star, and the similarity in these abundances for the bulge and disc PNe indicates that they started off with very similar

metallicities. However, given the inherent uncertainty in CEL abundances, a much larger survey, allowing for lower statistical errors and a more complete correction for selection effects, is recommended. A major uncertainty is the initial abundances of C and N for the bulge PNe.

Recent work on the abundances of the Galactic bulge population by van Loon et al. (2003) is interesting in light of our findings. Using near- and mid-IR data – which allows one to study the more obscured regions forbidden to optical studies – they studied the inner 1.4 kpc of the Galaxy. The observed colour–magnitude diagrams were fit to reveal a population dominated by old stars ($\geqslant$7 Gyr), but an intermediate-age population (200 Myr–7 Gyr) and young stars ($\leqslant$200 Myr) were also detected. The metallicities of these stars were interpreted in terms of an early epoch of intense star formation forming the bulge, with more continuous star formation forming the disc, with accretion of subsolar metallicity gas from the halo. They suggested that the youngest stars are possibly caused by an increase in star formation triggered by a minor merger. There is a hint that the metallicity increases towards the inner bulge, but only slightly. Our PN abundance results are consistent with our having detected their old solar-metallicity population (the non-Type I PNe), as well as the intermediate-age and young stellar populations (the Type I PNe). However, we see no evidence for either the very low-metallicity (their [M/H]$= -0.5$) or super-metal-rich ([M/H] $= 0.5$) populations that they claim evidence for in the old stars. Neither do we find any difference between our metallicity distributions for the bulge and disc populations. Allen, Carigi & Peimbert (1998) described a model for the chemodynamical evolution of the disc of our Galaxy, and (including some selection effects) predicted various PN-related parameters – such as the abundance gradients for the different PN types – which were compared with published data. They found that the best-fitting models resulted from assuming that not all intermediate-mass stars become PNe, with a fraction that decreases with mass (e.g. <30 per cent at <1 M$_\odot$). A result of this would be a reduction (relative to slightly higher mass stars) in the numbers of low-mass and low-metallicity stars that become PNe, just as found for our bulge PN sample, and there are also no very low-metallicity disc PNe in the KB94 sample. This is encouraging support for their model, although we do not account for all selection effects in our DFs, and do not divide our sample into the same range of types.

Finally, the B-star studies of Rolleston et al. (2000) indicate that abundances along the disc of the Galaxy increase with decreasing galactocentric radius, with a gradient of -0.07 dex kpc^{-1} for O and C and -0.09 dex kpc^{-1} for N, and much flatter at -0.04 dex kpc^{-1} for N/O, which they find agrees with the H II region results, and for O is similar to the gradient derived from PNe (e.g. Maciel, Costa & Uchida 2003). Bulge PN abundances, if they followed the trend, should then exceed the disc values; neither our own nor other bulge PN abundance surveys have found this behaviour. The bulge PN abundances are the same as for the local disc PNe, being about 0.5 dex lower than the extrapolated gradient at $R_G = 0$ for oxygen. This agrees with some results from H II regions.[7]

ACKNOWLEDGMENTS

We thank Q. A. Parker for his help during the observations, Ian Howarth for advice on statistics, and especially J. Köppen for many fruitful and encouraging discussions. KME was supported by a Research Studentship Award from PPARC, and by the Polish National Committee for Scientific Research under grant no. 2-P03D-005-16.

[7] It is interesting that, according to abundances derived for three H II regions by Afflerbach et al. (1997) around $R_G = 0$, this H II region gradient for N, S and O seems to extend right into the Galactic centre region.

REFERENCES

Acker A., Raytchev B., Köppen J., Stenholm B. R., 1991, A&AS, 89, 237
Acker A., Ochsenbein F., Stenholm B., Tylenda R., Marcout J., Schohn C., 1992, Strasbourg–ESO Catalogue of Galactic Planetary Nebulae. European Southern Observatory. Garching
Adams S., 1982, PhD thesis, University College London
Afflerbach A., Churchwell E., Werner M. W., 1997, ApJ, 478, 190
Alexander J., Balick B., 1997, AJ, 114, 713
Allen C., Carigi L., Peimbert M., 1998, ApJ, 497, 247
Allende Prieto C., Lambert D. L., Asplund M., 2001, ApJ, 556, L63
Aller L. H., 1956, Gaseous Nebulae. Chapman and Hall, London
Aller L. H., Keyes C. D., 1987, ApJS, 65, 405
Aggarwal K. M., 1983, ApJS, 52, 387
Becker S. A., Iben I., Jr, 1979, ApJ, 232, 831
Becker S. A., Iben I., Jr, 1980, ApJ, 237, 111
Benjamin R. A., Skillman E. D., Smits D. P., 2002, ApJ, 569, 288
Brocklehurst M., 1971, MNRAS, 153, 471
Brocklehurst M., 1972, MNRAS, 157, 211
Butler K., Zeippen C. J., 1994, A&AS, 108, 1
Cahn J. H., Kaler J. B., Stanghellini L., 1992, A&AS, 94, 399
Ciardullo R., Jacoby G. H., 1992, ApJ, 388, 268
Cuisinier F., Maciel W. J., Köppen J., Acker A., Stenholm B., 2000, A&A, 353, 543
De Marco O., 1997, PhD thesis, University College London
De Marco O., Crowther P. A., Barlow M. J., Clayton G. C., de Koter A., 2001, MNRAS, 328, 527
Dopita M. A., Henry J. P., Tuchy I. R., Webster B. L., Roberts E. H., Byun Y.-I., Cowie L. L., Songaila A., 1990, ApJ, 365, 640
Durand S., Acker A., Zijlstra A., 1998, A&AS, 132, 13
Edvardsson B., Anderson J., Gustafsson B., Lambert D. L., Nissen P. E., Tomkin J., 1993, A&A, 275, 101
Escudero A. V., Costa R. D. D., 2001, A&A, 380, 300
Exter K. M., 2000, PhD thesis, University of St Andrews
Fagotto F., Bressan A., Bertelli G., Chiosi C., 1994, A&AS, 105, 39
Feigelson E. D., Nelson P. I., 1985, ApJ, 293, 192
Feltzing S., Gilmore G., 2000, A&A, 355, 949
Greggio L., Renzini A., 1990, ApJ, 364, 35
Grevesse N., Sauval A. J., 1998, Space Sci. Rev., 85, 161
Henry R. C. B, 1989, MNRAS, 241, 453
Henry R. B. C., 1998, in Friedli D., Edmunds M., Robert C., Drissen L., eds, ASP Conf. Ser. Vol. 147, Abundance Profiles: Diagnostic Tools for Galaxy History. Astron. Soc. Pac., San Francisco, p. 59
Howarth I. D., 1983, MNRAS, 203, 301
Howarth I. D., Murray J., Mills D., Berry S., 1998, Starlink User Note 50.12
Hummer D. G., Storey P. J., 1987, MNRAS, 224, 801
Iben I., Renzini A., 1983, ARA&A, 21, 271
Johnson C. T., Kingston A. E., 1990, J. Phys. B, 23, 3393
Keenan F. P., Aller L. H., Bell K. L., Hyung S., McKenna F. C., Ramsbottom C. A., 1996, MNRAS, 281, 1073
Keenan F. P., Hibbert A., Conton E. S., Ojha P. C., 1993, Phys. Scr., 48, 129
Kingdon J., Ferland G., 1995, ApJ, 442, 714
Kingsburgh R. L., Barlow M. J., 1994, MNRAS, 271, 257
Kingsburgh R. L., English J., 1992, MNRAS, 259, 635
Liu X.-W., Luo S.-G., Barlow M. J., Danzier I. J., Storey P. J., 2001, MNRAS, 327, 141
Liu X.-W., Storey P. J., Barlow M. J., Danziger I. J., Cohen M., Bryce M., 2000, MNRAS, 312, 585
Maciel W. J., Costa R. D. D., Uchida M. M. M., 2003, A&A, 397, 667

Maciel W. J., Köppen J., 1994, A&A, 282, 436
Maciel W. J., Quireza C., 1999, A&A, 345, 629
Marigo P., 2001, A&A, 370, 194
Matteucci F., Brocato E., 1990, ApJ, 365, 539
Matteucci F., Romano D., 1999, Ap&SS, 265, 311
McWilliam A., Rich M. R., 1994, ApJS, 91, 749
Mendoza C., 1983, in Flower D. R., ed., IAU Symp. 103, Planetary Nebulae. Reidel, Dordrecht, p. 143
Mendoza C., Zeippen C. J., 1982a, MNRAS, 198, 127
Mendoza C., Zeippen C. J., 1982b, MNRAS, 199, 1025
Mendoza C., Zeippen C. J., 1983, MNRAS, 202, 981
Middlemass D., 1990, PhD thesis, University College London
Minniti D., Olszewski E. W., Liebert J., White S. D. M., Hill J. M., Irwin M. J., 1995, MNRAS, 277, 1293
Monk D. J., Barlow M. J., Clegg R. E. S., 1988, MNRAS, 234, 583
Morgan D. H., Parker Q. A., 1998, MNRAS, 296, 921
Mowlavi N., Meynet G., Maeder A., Schaerer D., Charbonnel C., 1998, A&A, 335, 573
Nussbaumer H., Rusca C., 1979, A&A, 72, 129
Nussbaumer H., Storey P. J., 1981, A&A, 99, 177
Osterbrock D. E., 1989, Astrophysics of Gaseous Nebulae and Active Galactic Nuclei. University Science Books, MMill Valley CA
Parker Q. A., 1997, in Kontizas M., Kontizas D. H., Morgan D. H., Vettolani G. P., eds, Proc. 2nd Conf. Working Group IAU Comm. 9, ASSL, Vol. 212. Kluwer, Dordrecht, p. 25
Peimbert M., 1978, In Terzian Y., ed., IAU Symp. 76. Reidel, Dordrecht, p. 215
Peimbert M., Serrano A., 1980, Rev. Mex. Astron. Astrofiz., 5, 9
Peña M., Torres-Peimbert S., Ruiz M. T., 1991, PASP, 103, 865
Péquignot D., Walsh J. R., Zijlstra A. A., Dudziak G., 2000, A&A, 361, L1
Pradhan A. K., 1976, MNRAS, 177, 31
Press W. H., Teukolsky S. A., Vetterling W. T., Flannery B. P., 1992, Numerical Recipes in Fortran, 2nd edn. Cambridge Univ. Press, Cambridge
Price C. M., 1981, ApJ, 247, 540
Ratag M. A., 1990, PhD thesis, University of Groningen
Ratag M. A., Pottasch S. R., Dennefield M., Menzies J. W., 1992, A&A, 255, 255
Ratag M. A., Pottasch S. R., Dennefeld M., Menzies J., 1997, A&AS, 126, 297
Rola C., Pelat D., 1994, A&A, 282, 199
Rolleston W. R. J., Smartt S. J., Dufton P. L., Ryans R. S. I., 2000, A&A, 363, 537
Rubin R. H., Martin P. G., Dufour R. J., Ferland G. J., Blagrave K. P. M., Liu X.-W., Nguyen J. K., Baldwin J. A., 2003, MNRAS, 340, 362
Samland M., Köppen J., Acker A., Stenholm B., 1992, A&A, 264, 184
Shaver P. A., McGee R. X., Newton L. M., Danks A. C., Pottasch S. R., 1983, MNRAS, 204, 53
Shortridge K. et al., 1999, Starlink User Note 86.17
Simpson J. P., Colgan S. W. J., Rubin R. H., Rickson E. F., Haas M. R., 1995, ApJ, 444, 721
Stafford R. P., Bell K. L., Hibbert A., Wijsundera W. P., 1994, MNRAS, 268, 816
Stasińska G., Richer M. G., McCall M. L., 1998, A&A, 336, 667
Stasińska G., Tylenda R., 1994, A&A, 289, 225
Torres-Peimbert S., Peimbert M., 1977, Rev. Mex. Astron. Astrofiz., 2, 181
Torres-Peimbert S., Dufour R. J., Peimbert M., Pe {n}a M., 1997, in Habing H. J., Lamers H. J. G. L. M., eds, IAU Symp. Vol. 180, Planetary Nebulae. Kluwer, Dordrecht, p. 281
Tsamis Y. G., Barlow M. J., Liu X.-W., Danziger I. J., Storey P. J., 2003, MNRAS, 345, 186
van den Hoek L. B., Groenewegen M. A. T., 1997, A&AS, 123, 305
van Loon J. Th. et al., 2003, MNRAS, 338, 857
Vílchez J. M., Esteban C., 1996, MNRAS, 280, 720
Walsh J. R., Dudziak G., Minniti D., Zijlstra A. A., 1997, ApJ, 487, 651
Walton N. A., Barlow M. J., Clegg R. E. S., 1993, in de Jonghe H., Habing H. J., eds, Galactic Bulges. Kluwer, Dordrecht, p. 337
Watson F. G., Gray P. M., Oates A. P., Lankshear A., Dean R. G., 1993, in Gray P. M., ed., ASP Conf. Vol. 37, Fibre Optics in Astronomy II. Astron. Soc. Pac., San Francisco, p. 171
Webster B. L., 1988, MNRAS, 230, 377
Wyse R. F. G., 1999, ApSS, 267, 145
Zeippen C. J., 1982, MNRAS, 198, 111
Zeippen C. J., Butler K., le Bourlot J., 1987, A&A, 188, 251

APPENDIX A: SELECTION EFFECTS WITH BRIGHTNESS

Most of our PNe are also in the catalogue of Acker et al. (1992) and were first discovered via emission-line surveys. Usually the discovery of a PN is dependent on its integrated or surface brightness (the latter more so for the resolved disc PNe). To search for biases in our derived abundances from brightness-based selection effects, we have looked for any trends in the important parameters T_e, n_e, A(O), A(N) and the N/O ratio with V magnitude, observed Hβ flux – F(H β) – and [O III] flux [the relative 5007-Å flux multiplied by F(Hβ)]. Relevant data were taken from Acker et al. (1999).

There is a slight trend for the Hβ and [O III] fluxes to decrease with n_e, a trend that is perfectly understandable. For the bulge PN, and to a lesser extent for the disc PN, there is also a slight decrease of the two flux indicators with increasing T_e(O III) – the hottest PN are fainter. For T_e(N II) the opposite if found; the hottest bulge PN are bright in [O III]. However, both of these trends are well within the scatter of the data and their errors. Considering also that we find no trends for the abundances with the brightness parameters, we believe that our abundance results are not (internally) dependent on brightness.

We have also compared the distributions of the brightnesses (above), angular size (for the disc PNe) and (for the bulge sample) stellar V magnitude for our PNe with those for all the bulge and disc PNe in the catalogue of Acker et al., treating a PN as a bulge object if so noted in the catalogue. We find that the DF for these parameters for our bulge sample agrees excellently with the catalogue as a whole. Therefore, in as much as that catalogue is a representative sample of bulge PNe for these parameters, so is our sample. For the disc PNe, the KB94 sample is noticeably shifted to the bright end of the all-PN distribution. Although there is no relationship between abundance and brightness *within* the KB94 disc PN sample, the fainter (e.g. larger and older and/or more distant) PNe are being selected against in our particular sample. These tests do not, however, exclude the possibility that there are particular types of PNe that are selected against because they are harder to find in the first place (see Section 5.1).

APPENDIX B: INTERNAL SELECTION EFFECTS

In this paper we have compared bulge and disc PN abundances, so we have searched through our data sets to find any differences between these two samples in the dependence of the abundances on T_e, n_e, line fluxes, spectral quality – S/N and errors for the important Balmer lines – excitation class, Galactic coordinates l and b, or angular size (information not derived from our data was taken from Acker et al. 1992). We found the following.

(i) As noted by Webster (1988), observed bulge PNe tend to be of lower excitation than disc PNe. In our samples there is a higher incidence of He II emission for the disc PNe, as was discussed previ-

ously in Section 3.1. This is because higher excitation PNe are more likely to be present in a sample of disc PNe as they tend to be older and larger, and being of lower surface brightness are more likely to be missed in the crowded bulge fields.

(ii) The 23 highest quality bulge PN spectra show a smaller scatter in T_e(O III) compared with the whole sample – by eye, about 7500–13 000 K compared with 5000–18 000 K – and the bulk of the objects lie at a lower mean T_e(O III), by 1000–2000 K. There is however only a 0.1 dex difference in the distribution of the two samples in A(O). For these highest quality PNe, the mean abundances and standard deviation values are the same, within the errors, as for the entire sample.

(iii) Among the disc PNe, 10 per cent are incompletely ionized, among the bulge PNe, 30 per cent.

This paper has been typeset from a TEX/LATEX file prepared by the author.